Quantification of the water content in synthetic glasses and natural melt inclusions using confocal Raman spectroscopy

By
Connor John Dalzell

A Thesis Submitted to
Saint Mary's University, Halifax, Nova Scotia
in Partial Fulfillment of the Requirements for
the Degree of Geology.

April 28th, 2017, Halifax, Nova Scotia

Approved: Dr. Jacob Hanley
Associate Professor
Department of Geology

Date: April 28th, 2017

Quantification of the water content in synthetic glasses and natural melt inclusions using confocal Raman spectroscopy

By

Connor John Dalzell

Abstract

The importance of water in controlling magmatic ore-forming processes cannot be understated. To accurately constrain the water content in these systems, the application of confocal 532 nm laser Raman spectroscopy was evaluated on silicate glasses of varying bulk composition and water content with a final goal of testing the method developed on hydrous melt inclusions from natural samples. Water derivation is ultimately based on the ratio between areas of the silicate region at 700-1250 cm^{-1} and the O–H region at ~3600 cm^{-1} of the Raman spectra. Calibration of this method was carried out using hydrous synthetic glasses of rhyolitic, dacitic, and trachytic compositions with a range in water contents (2.68 to 6.59 wt% H_2O). This study identified important steps for spectral treatment in the water quantification process, including baseline correction of the spectra and application of the frequency-temperature correction. The largest source of error for this determination was identified as a combination of glass sample heterogeneity and variations in the baseline correction of the spectra. The phenomenon of fluorescence, in coloured or impure glasses, obscures the water band and makes baseline corrections difficult. This was investigated through comparison of hydrous and anhydrous synthetic glasses of the same composition to evaluate a correction protocol, and the use of near-UV excitation sources to reduce fluorescence. Finally, this method was applied to natural, quartz-hosted melt inclusions from Late Paleozoic rhyolites from Southern New Brunswick. Ultimately, the method developed enables constraining of water content to within an average ~0.85 wt% accuracy for both synthetic glasses and natural melt inclusions. This is sufficient to differentiate between degassed vs. undegassed liquids, or melts trapped at contrasting crustal depths.

Date: April 28th, 2017

Acknowledgements

I am thankful to J. Webster, PhD (American Museum of Natural History, New York) and his PhD student, A. Iveson, for providing synthetic glass samples for our calibration. I thank J. Brenan, PhD (Dalhousie University, Halifax) for use of his laboratory and expertise in creating anhydrous glasses for our analysis of fluorescence. I also thank Sergey Mamedov, PhD (HORIBA Scientific, New Jersey) for his expert advice on Raman spectroscopy and for use of his 405nm UV spectrometer. I am grateful to Z. Zajacz, PhD (University of Toronto) for clarifying our understanding of Raman spectral treatments, and for participating as an external reviewer for this paper. Finally, I would like to thank J. Hanley, PhD (Saint Mary's University, Halifax) for his tutelage and constant support of the project, and for providing natural melt samples for our analysis.

Table of Contents

List of Figures

List of Tables

1.0 Introduction

The water content of silicate magmas plays an important role in the formation of magmatic–hydrothermal ore deposits through exsolution as a magmatic volatile phase, and influences an array of physicochemical properties such as viscosity, the composition of mineral assemblages that form during crystallization, and the temperatures and pressures of phase changes (Burnham, 1979, Lange, 1994, Ingerson, 1950). In addition, water is the most abundant volatile that gets released from siliceous magmas as they start to crystalize, which is the primary mechanism for ore fluid transportation (Hedenquist & Lowenstern, 1994). As such, it is crucial to have a precise constraint on water content, such that the degassing and crystallization histories of ore-forming magmas may be derived. Melt inclusions provide the best-preserved samples for determining water content in silicate melts. Hence, an analysis of melt inclusions provides an opportunity to investigate the evolution of magmatic systems (Thomas, 1994, Thomas et al., 2006, Zajacz et al., 2005). In doing so, it may be possible to predict the most productive (i.e., metal-fertile) magmatic events.

1.1 Analytical methods for water determination

Karl-Fisher titration is conventionally used to determine bulk water content in solid materials. The relatively small size of melt inclusions, however, makes this method impractical (Chabiron & Pironon, 2004). Several other micro techniques have been developed to quantify water content in glasses, such as electron microprobe and ion microprobe analysis. A great disadvantage of these methods is the need to have inclusions exposed at surface, or to have doubly-polished sections in the case of IR spectroscopy. This is not a problem for the analysis of bulk glasses, but may prove difficult for melt inclusions <50um in diameter (Behrens et al., 2006). In addition, methods like ion microprobe can

only provide an of estimate total water content, due to their inability to detect hydrogen. In these cases, water content is measured by subtracting total detected elements from 100% (Chabiron & Pironon, 2004). Even using standards with known water contents for calibration, the analytical uncertainty for these methods is typically ~0.5 wt% (Behrens et al., 2006).

1.2 Raman spectroscopy

The determination of water content in silicate glasses has been well described using Raman spectroscopy (Thomas et al., 2006, Thomas 2000; Chabiron et al. 2004). This technique relies on measuring the inelastic scattering of laser light as it interacts with molecular vibrations (bonds) within a sample. The resulting shift in wavelength of the incident laser light, measured as wavenumber, provides information about the type of molecular bonds within the sample.

There are two areas of the Raman spectra that are important in determining the water content of hydrous silicate glasses. The "T-O band" is a low-wavenumber region (located at ~470–570 cm^{-1} or ~850-1250cm^{-1}) which corresponds to the vibration of various T–O bonds within the sample (where "T" represents fourfold coordinated cations, and "O" represents bridging or non-bridging oxygen atoms) (Zajacz et al., 2005 and Mercier et al., 2009). The "water band" is a high-wavenumber region (located at ~3600cm^{-1}) that represents OH stretching vibrations from hydroxyl groups and H_2O molecules (Mercier et al., 2009). Both the water band and the T-O band (from ~850-1250cm^{-1}) are visualized in the Raman spectra of *Figure 1*.

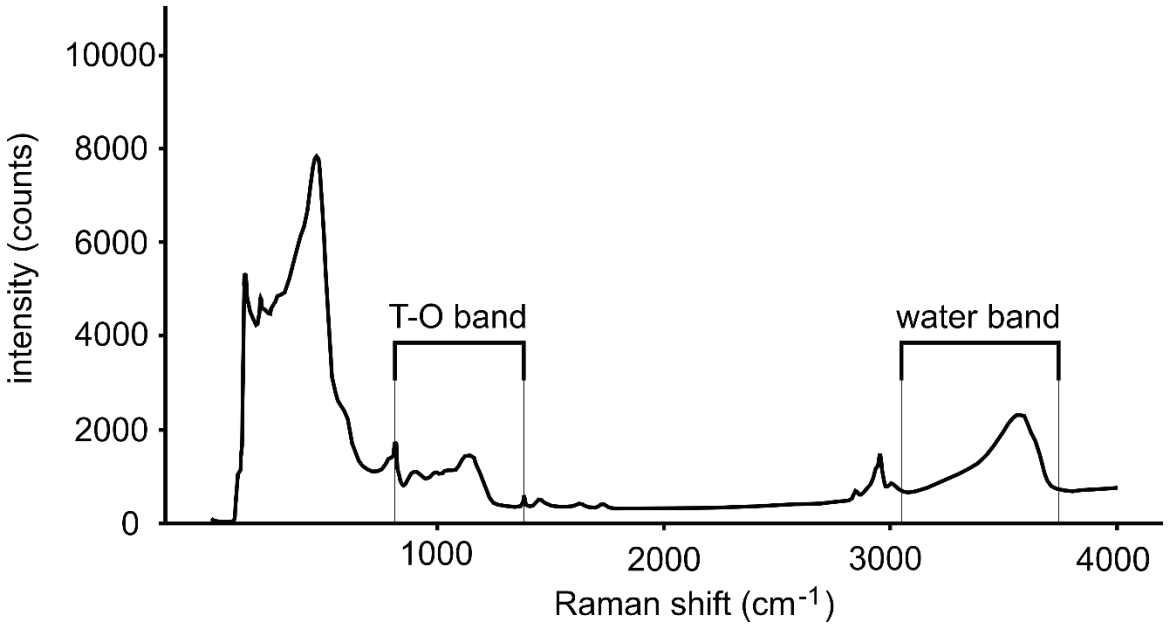

Figure 1: Uncorrected Raman spectra of a hydrous silicate glass (sample 1-8-6 B) highlighting the T-O region (from ~850-1250cm^{-1}) and water-band region (located at ~3600cm^{-1}).

1.2.1 Raman spectroscopic features of water within glasses and minerals

It is important to recognize that the shape/area of the T-O band and the water band are not independent of composition. Hence, different features can be observed in Raman spectra based on the molecular structure and composition of the glass. For instance, the shape of the water band region (~3600cm^{-1}) is highly dependent on the concentration of water dissolved in the glass. This region becomes much higher and broader as the amount of water increases, and becomes short and narrow as it decreases (Le Losq 2012). The intensity of the Raman peak in this region is directly proportional to the H_2O concentration of the sample, and is largely unaffected by the anhydrous composition of the glass (Severs et al., 2007).

The T-O area (~470–570 cm^{-1} or ~850-1250cm^{-1}), in contrast, is relatively unaffected by the water content of the sample. Instead, the shape and position of this region depends on the SiO_2 content and other anhydrous components of the glass. For instance, the presence of 3-6 membered rings of tetrahedra in the aluminosilicate network is responsible for the large peak at ~500cm^{-1} (See *Figure 1*). The peak near 800cm^{-1} is caused by Si-O stretching vibrations in samples with up to 60–65 wt% SiO2 (Le Losq 2012). Iron molecules create a peak at 940–970 cm^{-1}, which is attributed to vibrating Fe–O–Si bonds (Zajacz et al., 2005). The band at 586 cm^{-1} has been attributed to defects in the glass structure, while the 776 cm^{-1} band has is caused by T–O–T bending vibrations (Severs et al., 2007). Finally, the broad region between 850 and 1250cm^{-1} is influenced by symmetric and asymmetric stretching in the Al-Si-O network (where "O" includes both bridging and non-bridging oxygen atoms). (Le Losq 2012). This demonstrates how the anhydrous composition of the glass influences the T-O region.

1.2.2 T-O area normalization

Previous works have found a strong correlation between the water content of a glass and the area ratio between the water band and the T-O band (either at ~470–570 cm^{-1} or ~850-1250cm^{-1}) (Thomas 2000, Mercier et al., 2009, Le Losq 2012). Normalizing these regions works as an internal calibration to accurately derive the water content represented by the ~3600cm^{-1} region. Although some studies have derived water content using the height/area of the water peak alone, it is often quite difficult to determine absolute Raman heights or areas (Mercier et al., 2009). Peak area ratios are also used rather than peak intensities (heights) to eliminate the need for multiple calibrations (due to long-term instability of the Raman laser) (Severs et al., 2007). In addition, a variety of factors can influence the shape and area of the water band, such as the reflectance and chemistry of the sample, and the depth of the analyzed volume below the samples surface (Zajacz et al., 2005, Mercier, et al., 2009, Behrens et al., 2006). Therefore, it is necessary to calibrate the water band using an internal standard.

1.2.3 Advantages and disadvantages of Raman spectroscopy

Raman spectroscopy is capable of analyzing water content in glasses and melt inclusions through a concentration range of 0 to 20 wt% H_2O (Thomas, 2000). Additionally, there are several advantages to using Raman spectroscopy over other methods for the analysis of silicate melt inclusions and glasses. These include a high-spatial resolution (1-2 μm), the ability to analyze inclusions at different depths, a non-destructive character, and minimal sample preparation (i.e. no need for doubly-polished thin sections like FTIR, which proves difficult for melt inclusion analysis) (Le Losq, 2012, Thomas et al., 2006 Zajacz et al., 2005).

It is important to note that there are several disadvantages to using this analytical technique. For instance, Raman analysis can be limited by fluorescence, which will obscure the Raman scattering of target materials. Fluorescence can be caused by trace elements, colouration, or defects in the crystal lattice (Campbell et al., 1986). Additionally, the depth of melt inclusions, in outcrop or prepared sample, may also influence water content determination. Near-surface melt inclusions may be subject to weathering, which causes water re-equilibration with the atmosphere. Deeply buried melt inclusions within the sample will report a measured water content ~10% less than normal when exceeding a depth of ~120 μm. Finally, variations in the size and shape of the water band (caused by instrumental effects, spectrometer settings, and the depth of the analyzed material below the surface) means that a calibration established for one instrument can not be transferred to another. In order to use this technique, each laboratory must run its own calibration procedure (Behrens, et al., 2006).

1.3 Approach

By analyzing a suite of hydrous silicate glass, a calibration curve may be generated relating measured water content to known water content. Once the Raman has been calibrated, this method will be applied to natural melt inclusions from the Late Paleozoic rhyolites of Southern New Brunswick.

2.0 Geological setting

The Late Devonian-Pennsylvanian Harvey volcanic suite occurs on the eastern edge of the Maritimes basin, 55 km southwest of Fredericton, New Brunswick (see *Figure 2*) (Payette & Martin, 1986, Gray et al., 2011). The Harvey Fm. occurs stratigraphically at the base of

the Maritimes basin, which is a 12km thick succession that formed during the mid-Devonian in the final stages in the growth of Pangea. Stratigraphic and petrological data suggests that the Piskahegan Formation, deposited at 363.4 ± 1.8 Ma, is synchronous with the Harvey Formation. For example, some of the Harvey volcanic rocks can be correlated with those of the Mount Pleasant caldera, Piskahegan Group.

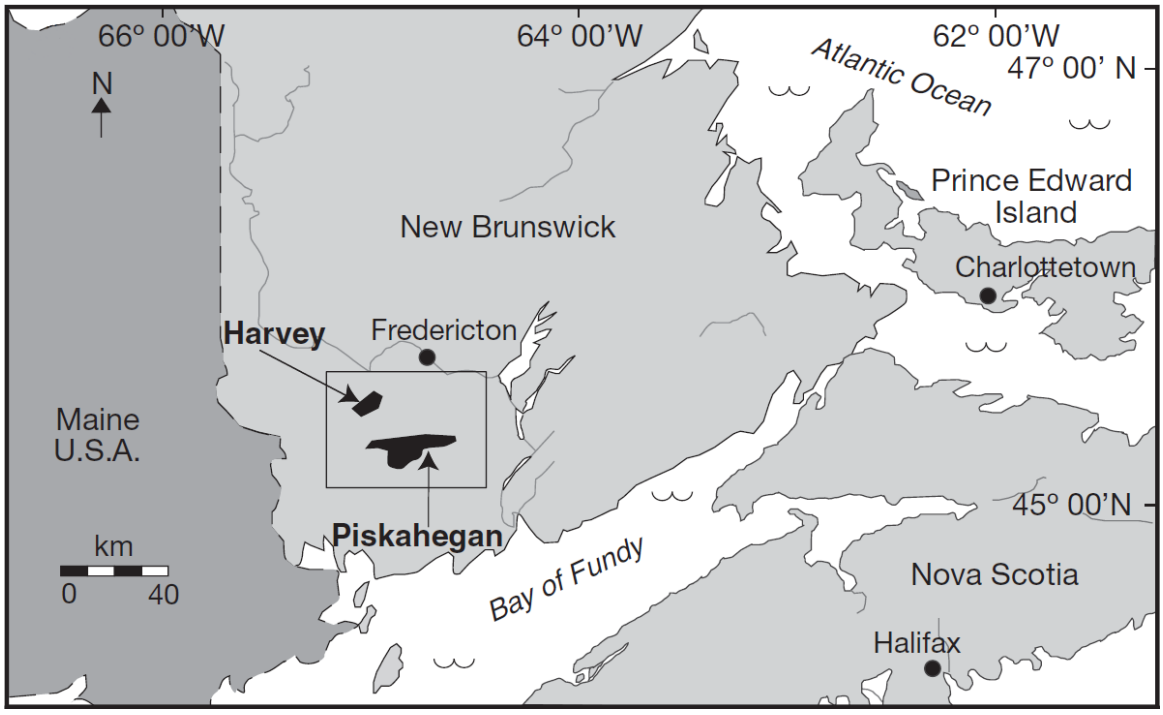

Figure 2: Location of the Harvey and Piskahegan Formation in Southern New Brunswick, Canada (modified from Gray et al., 2011).

2.1 Regional geology

The Maritimes Basin has undergone four discrete magmatic events, controlled by faulting, basinal extension, and repeated basin subsidence from the Middle Devonian to the late Tournaisian (Gray et al., 2011). During the Carboniferous, the Maritimes Basin underwent an extensional phase which resulted in large-scale normal/strike-slip faults, with numerous associated small grabens. To the north-northwest, the Harvey formation is limited by the Fredericton-Norumbega fault, which is a major regional strike-slip fault (Payette & Martin, 1986).

The folded and faulted Harvey Formation was likely derived from partial melting of continental crust during a rifting (extensional) phase of the Maritimes Basin, in response to an influx of mantle-derived basic magmas (Payette & Martin, 1986). The Harvey volcanic unit is primarily composed of subaerially deposited, welded ash-fall/ash-flow volcanic tuff (Bottomley, 1984). The Harvey Formation is situated on the lower, northwest limb of a large northeast-plunging syncline, and is overlain by successive red beds of the Mississippian-Pennsylvanian Shin Formation (Bottomley, 1984, Payette & Martin, 1986). It is underlain by Silurian metasediments (Payette & Martin, 1986).

2.2 Local geology

The Harvey volcanic suite consists of three units: York Mills, Cherry Hill, and Harvey Mountain.

York Mills comprises felsic volcanogenic sediments, minor ash-flow, and laminated rhyolite (Payette & Martin, 1986). Bands of lapilli tuff are also found interbedded

throughout the unit. Sedimentary rocks (red sandstone and siltstone) are the dominant rock type at York Mills (Payette & Martin, 1986, Gray et al., 2011). Detrital grains within the sandstone usually consist of quartz and feldspar phenocrysts, with minor fragments of rhyolite. The itself deposit is roughly 60m thick (Payette & Martin, 1986).

The Cherry Hill unit forms an assemblage of felsic volcanic rock, including volcanogenic sediments (approximately 10m thick), two sheets of ash-flow tuff (5 and 100m thick), volcaniclastic sediments (approximately 20m thick), quartz-feldspar porphyry, and ash-fall tuff (approximately 40m thick) (Harvey, 2016, Payette & Martin, 1986). The quartzfeldspar porphyry is host to ~20% phenocrysts of euhedral quartz and feldspar, up to 3 mm in diameter. Occurrences of glass are sometimes preserved in these quartz phenocrysts. The quartz-feldspar porphyry contains a groundmass of devitrified welded shards, and is thought to correspond to the most densely welded portion of an ash-flow tuff (Gray et al., 2011, Payette & Martin, 1986). The base of Cherry Hill is composed of volcanogenic sediments and lithic tuff (Payette & Martin, 1986). Cherry Hill volcanics lie unconformably over black slate, argillite and graywacke of Pre-Carboniferous age, and are overlain by red shale, conglomerate and sandstone (Harvey, 2016).

The Harvey Mountain Formation consists dominantly of laminated rhyolite, with minor ash-fall tuffs and pyroclastic breccia (Harvey, 2016, Payette & Martin, 1986). These rhyolites have an aphanitic texture, with well-defined alteration represented by gray-green layers of coarse spherulites (3–4 mm across) (Payette & Martin, 1986, Gray et al., 2011). Glass is found in the rhyolite, being replaced by illite and quartz (Gray et al., 2011). The deposit is estimated 75-150m thick (Payette & Martin, 1986). Fluorite is often found

disseminated within the felsic rocks in this outcrop, with minor hematite, quartz, white mica, and clay minerals (Harvey, 2016). The presence of tridymite in outcrop suggest a high emplacement and devitrification temperature of ~870-900^{o}C (Payette & Martin, 1986).

The coeval Piskahegan Formation represents a caldera sequence with preserved exocaldera, intracaldera, and late caldera fill structures. Large melt inclusions, hosted in quartz phenocrysts, are found preserved in the Bailey Rock rhyolites within the exocaldera sequences. The Bailey Rock unit is characterized by quartz-feldsparphyric lava flows, containing K-feldspar phenocrysts, quartz, plagioclase, and hornblende pseudomorphs (Gray et al., 2011).

2.3 Mineralization

The rhyolitic rocks of the Harvey and Piskahegan contain uranium mineralization (Gray et al., 2011). U-mineralization occurs as pitchblende, with associated pyrite, arsenopyrite, molybdenite, quartz, and fluorite (Payette & Martin, 1986). The mineralization style is defined as caldera or volcanic related uranium, which is thought to be either synvolcanic or epigenetic, and is highly structurally controlled (Gray et al., 2011). Interest in the region started in 1954, with the discovery of these uranium occurrences (Payette & Martin, 1986). Although several test holes have been drilled, no economically significant deposits were found, and no mining of this formation has taken place (Bottomley, 1984, Payette & Martin, 1986). Recently, exploration of the Harvey Fm. has found uranium concentrations grading 0.24-0.45% U_3O_8 over 1.2 and 0.6 meters respectively (Gray et al., 2011).

2.4 Water content

Glasses preserved in quartz and feldspar at Cherry Hill, Harvey Mountain, and Bailey Rock were analyzed by Gray et al., (2011) via electron microprobe (difference in oxide totals measured compared to 100%). The water values derived from their analysis will be used in comparison to our Raman analysis of melt inclusions from Cherry Hill.

3.0 Methods

A suite of hydrous silicate glasses with a wide compositional range and known water contents will be analyzed via Raman spectroscopy. The resultant spectra will undergo spectral treatment to allow for calculation of true T-O and water band areas. The area ratio of these two regions will then be used in an equation to quantify the water content represented by the spectra. A comparison of known vs. calculated water contents will ultimately be used to generate a calibration line for use on natural samples. This paper follows the work of Zajacz et al. (2005) as a basis for the various steps of analysis, and attempts to improve on them and explore their validity further.

3.1 Glass samples

Synthetic glasses with a range of hydrous and anhydrous chemistry were provided by Dr. James Webster of the American Museum of Natural History. Previous works by Webster et al., (2011 and 2014) had constrained a precise estimate of water content via FTIR. These glasses were also used by Zajacz et al. (2005) in his determination of water content using Raman spectroscopy. The glasses range from 1-9wt% H_2O, 58-75wt% SiO_2, and have an A/NK of 0.9-1.1. Overall, the glasses are rhyolitic, trachytic and dacitic in composition. The compositional data for these glasses are recorded in *Table 1*.

As mentioned previously, the fluorescence of samples during Raman analysis is a major disadvantage of the method as it obscures the Raman scattering of target materials. A novel method to account for fluorescence is to create synthetic analogues of the fluorescent glasses, minus the water content. The resulting anhydrous Raman spectra may be subtracted from the hydrous spectra, leaving only the non-fluorescent components behind. As such, several anhydrous equivalents of Dr. Webster's glass were created. Samples 1-10-15 A and T 1-4-13 were selected for replication as they both vary in composition from each other and show strong levels of fluorescence. Samples were synthesized using carbonate/Fe_2O_3 equivalents at Dalhousie's Earth Sciences laboratory with the help of Dr. James Brennan (See *Tables 2* and *3*). Samples were calcined at 1400^{o}C for 3 days, and extracted for mounting and polishing.

Both the hydrous and anhydrous equivalents of Dr. Webster's glass were mounted in transparent resin and polished before Raman analysis. This provided ease of use in handling the glass chips, which were only a few mm across, and a fresh surface required for Raman analysis. Samples were mounted using a Buehler Electro-hydraulic mounting press (SimpliMet™ 3000 Series) in Buehler TransOptic resin. Samples were subsequently polished using 2000grt sandpaper and 1μm diamond paste.

Table 1: Compositional data, water content, and fluorescence levels for standard glasses (values in wt%)

Sample no.	1-08-06B	1-09-10A	1-09-10B	1-10-01A	1-10-01B	1-10-02A	1-10-02B	1-10-15A	1-10-15B	1-10-15C	1-13-10	1-13-21	1-14-09A	1-15-04 T	1-4-14 T	1-5-6
glass type[a]	R	R	R	R	R	R	R	R	R	R	D	D	D	D	T	T
SiO_2	75.27	71.70	74.09	75.80	75.70	74.07	74.72	73.39	73.16	72.98	65.68	66.85	64.51	68.52	58.02	59.55
Al_2O_3	12.67	12.33	12.26	12.92	12.84	12.95	12.95	12.12	12.31	12.38	14.37	14.46	14.15	14.84	20.94	18.45
Na_2O	4.43	4.05	4.22	4.57	4.50	4.81	4.61	3.87	4.07	4.10	4.34	4.86	4.86	4.63	6.92	6.00
K_2O	4.57	4.30	4.43	4.74	4.76	4.90	4.87	4.77	4.48	4.48	0.86	0.98	0.99	0.95	5.56	5.30
FeO	0.00	0.00	0.00	0.00	0.00	0.00	0.00	1.04	1.16	1.08	3.38	2.48	3.10	2.91	1.48	1.19
S	0.02	0.00	0.00	0.00	0.00	0.01	0.01	0.11	0.10	0.10	0.01	n.a.	n.a.	0.00	0.01	0.00
TiO_2	-	-	-	-	-	-	-	-	-	-	0.39	0.38	0.40	0.37	0.12	0.12
MnO	-	-	-	-	-	-	-	-	-	-	0.16	0.20	0.12	0.24	0.06	0.03
MgO	-	-	-	-	-	-	-	-	-	-	0.83	0.92	1.03	0.85	0.16	0.13
CaO	-	-	-	-	-	-	-	-	-	-	3.47	3.55	3.48	3.68	1.54	1.24
P_2O_5	-	-	-	-	-	-	-	-	-	-	0.14	0.12	0.14	0.15	0.04	0.01
Cl	-	-	-	-	-	-	-	-	-	-	0.01	0.71	1.06	0.19	0.88	0.92
F	-	-	-	-	-	-	-	-	-	-	0.02	0.02	0.01	0.05	0.75	0.65
CO_2	0.07	0.00	0.05	0.10	0.09	0.03	0.02	0.03	0.04	0.04	14.50	4.50	0.00	15.80	0.16	0.19
H_2O	2.68	5.94	4.32	2.27	2.45	3.93	5.35	4.25	3.98	3.37	5.99	6.59	5.44	3.38	5.07	5.34
Total	96.95	92.38	95.01	98.03	97.80	96.74	97.17	95.31	95.27	95.12	93.66	95.35	93.65	97.32	101.71	99.12
N/NK	0.60	0.59	0.59	0.59	0.59	0.60	0.59	0.55	0.58	0.58	0.88	0.88	0.88	0.88	0.65	0.63
A/NK	1.04	1.09	1.04	1.02	1.02	0.98	1.01	1.05	1.07	1.07	1.00	0.93	0.92	0.97	1.04	1.03
fluorescence	no	no	no	no	no	no	no	yes	yes	yes	no	yes	no	yes	yes	yes

[a] where R= rhyolite, D= dacite, and T= trachyte

- = not analyzed or calculated.

Table 2: Compositional data required to generate an anhydrous melt of equivalent composition

Sample no.	1-10-15 A				
	Compositional data[1]	normalised to 100%[2]	carbonate/Fe_2O_3 equivalents[3]	milligram conversion[4]	weighed[5]
SiO_2	73.4	77.1	77.1	771	771
Al_2O_3	12.1	12.7	12.7	127	127
Na_2O	3.87	4.07	6.95	69.5	70.0
K_2O	4.77	5.01	7.35	73.5	73.8
FeO	1.04	1.09	1.21	12.1	12.4
TiO_2	-	-	-	-	-
MnO	-	-	-	-	-
MgO	-	-	-	-	-
CaO	-	-	-	-	-
anhydrous sum	95.19	100	-	-	-

Sample no.	T 1-4-14				
	Compositional data[1]	normalised to 100%[2]	carbonate/Fe_2O_3 equivalents[3]	milligram conversion[4]	weighed[5]
SiO_2	58.0	61.2	61.2	612	613
Al_2O_3	20.9	22.1	22.1	221	221
Na_2O	6.92	7.30	12.48	125	125
K_2O	5.56	5.86	8.60	86.0	86.0
FeO	1.48	1.56	1.74	17.4	17.3
TiO_2	0.12	0.13	0.13	1.27	1.30
MnO	0.06	0.06	0.06	0.63	0.50
MgO	0.16	0.17	0.17	1.69	1.40
CaO	1.54	1.62	2.90	28.99	29.20
anhydrous sum	94.80	100	-	-	-

- = not analyzed or calculated

[1]composition of the hydrous melt in oxide wt%

[2]composition of the "hydrous melt" without water and normalized to 100%

[3]amount of solids required to generate an anhydrous melt of equivalent composition (in grams)

[4]amount of solids required to generate an anhydrous melt of equivalent composition (in milligrams)

[5]amount of solids weighed out during actual measuring

Table 3: True compositional data of anhydrous vs. hydrous glass samples via SEM (values in wt%)

Sample #	1-10-15 A		T 1-4-14	
Sample type	Hydrous	Anhydrous	Hydrous	Anhydrous
SiO_2	73.39	77.7	58.02	61.05
Al_2O_3	12.12	14.69	20.94	24.4
Na_2O	3.87	2.34	6.92	6.32
K_2O	4.77	4.18	5.56	5.29
FeO	1.04	1.08	1.48	1.35
TiO_2	0	0	0.12	0
MnO	0	0	0.06	0
MgO	0	0	0.16	0
CaO	0	0	1.54	1.6
Total	95.19	99.99	94.8	100.01

3.1.1 Quality control: heterogeneity

It is important to recognize that glass samples may not be completely homogeneous. As such, Raman analysis on one region of the glass may produce different spectra than another, which will ultimately lead to a different derived water content. In order to quantify the effect of heterogeneity on the resultant spectra/water determination, multiple analyses were run on the same glass in different regions for samples 1-8-6B, 1-14-9 A, and T 1-5-6 (to represent our full compositional range of glasses, being rhyolitic, dacitic, and trachytic).

3.2 Raman spectroscopy

Spectra were captured using a Horiba Jobin-Yvon LabRam HR spectrometer, equipped with LabSpec v.6.3.40.4 software. The spectrometer was outfitted with a 100mW, 532nm Nd-YAG diode laser (Toptica Photonics), a 100x Olympus MPlanN objective (0.21 nm WD), and a Synapse charge-coupled device (CCD; Horiba Jobin-Yvon) detector, which was cooled below -50^{o}C to minimize dark current effects. Frequency calibration of the spectrometer was carried out using pure silicon.

There are a variety of settings on the spectrometer that may be adjusted to produce the highest-resolution Raman spectra. These include the confocal hole size, grating, laser power, number of accumulations, and acquisition time. Thus, these parameters were tested iteratively to produce the highest-resolution spectra while (1) remaining time effective, (2) reducing fluorescence levels of affected glasses and (3) avoiding "flooding" of the Raman detector. Note that some settings, such as the 100x objective, were chosen outright to optimize the calibration procedure for small, natural melt inclusions (a few μm across) rather than bulk glass samples.

The effects of each setting on the resultant spectra, and the resultant "optimal settings" are reviewed in the Results/Discussion section of this paper. Once found, these settings were used henceforth during spectral acquisition, and are as follows:

1. 100μm confocal hole diameter
2. 1800 grooves/nm grating
3. 4 accumulations
4. 20 second acquisition time
5. 100% laser power

3.3 Spectral treatment

In order to accurately derive water content from acquired spectra, the deleterious effects of fluorescence, instrumental effects, and environmental factors (such as temperature and humidity) must be accounted for. As outlined by Zajacz et al. (2005), and Le Losq (2012), the raw spectra first underwent baseline removal and frequency-temperature correction before spectral deconvolution took place (i.e. fitting the spectra to a function to find the areas of the T-O and water band).

3.3.1 Baseline removal

An important step in the internal calibration process is the removal of the spectral background. This background is present in the T-O and water band regions of the spectra, and is thought to be caused by fluorescence, luminescence, and reflectance of the sample under laser radiation (Chabiron, 2004, Zajacz et al., 2005). The degree in which these parameters affects the background level of the spectra depends, in part, on acquisition parameters and the structure and chemistry of the sample. As such, the baseline correction

procedure is unique to each individual Raman spectra, and is thus often based on empirical considerations (Le Losq, 2012).

A number of methods have been proposed to facilitate the baseline correction of Raman spectra. For instance, Zhang et al. (2009) developed an algorithm-based software which uses Wavelet transforms to identify peak maxima and correct the spectral background. However, such algorithm-based corrections may become problematic when analyzing glasses, as the broad and asymmetric nature of their Raman peaks may cause a misalignment of the peak maxima (Le Losq, 2012). Another method was proposed by Behrens et al. (2006), involving a set of nine invariant nodes that was used to draw the baseline for all glasses. Although this eliminated some ambiguity in the experiment, the method became highly dependant on the structure and chemistry of the glass, as these affect the prominence of peaks in key areas (500 cm^{-1} and 1000 cm^{-1}). As such, several calibrations were employed (dependant on the silica content of the glass), adding to the complexity of this method (Le Losq, 2012).

A simple method for baseline subtraction was employed by Zajacz et al., (2005), which involves the linear extrapolation of the baseline from the flat signal region from 1,250– 1,850 cm^{-1} (See *Figure 3*). According to Zajacz et al., (2005) this method provides both accurate and reproducible results. As such, the baseline correction procedure proposed by Zajacz et al., (2005) was carried out for all spectra using Fityk software. Fityk is a nonlinear peak-fitting program developed by Wojdyr, M. (2010). It is primarily used to fit peaks using bell-shaped functions (Gaussian, Lorentzian, etc.), but it also has several built-in tools that are useful for Raman analysis. One such function is the “manual baseline

subtraction tool", which was the primary implement used for all baseline corrections in this study (See *Figure 4*).

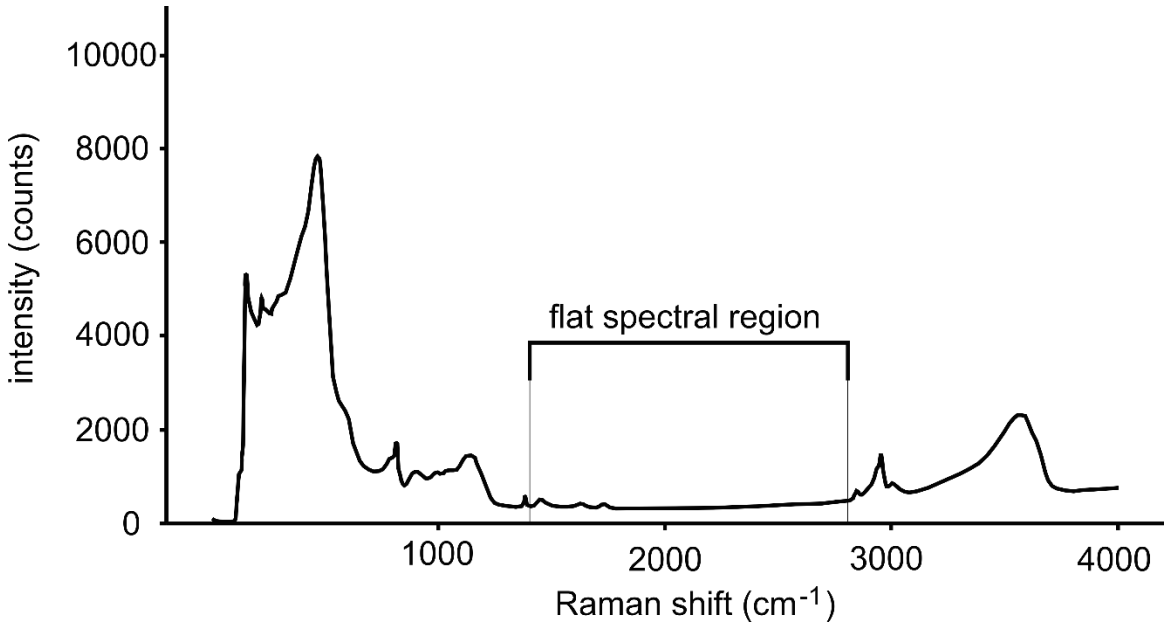

Figure 3: The flat signal region from 1,250–1,850 cm^{-1}described in Zajacz et al. (2005) baseline correction.

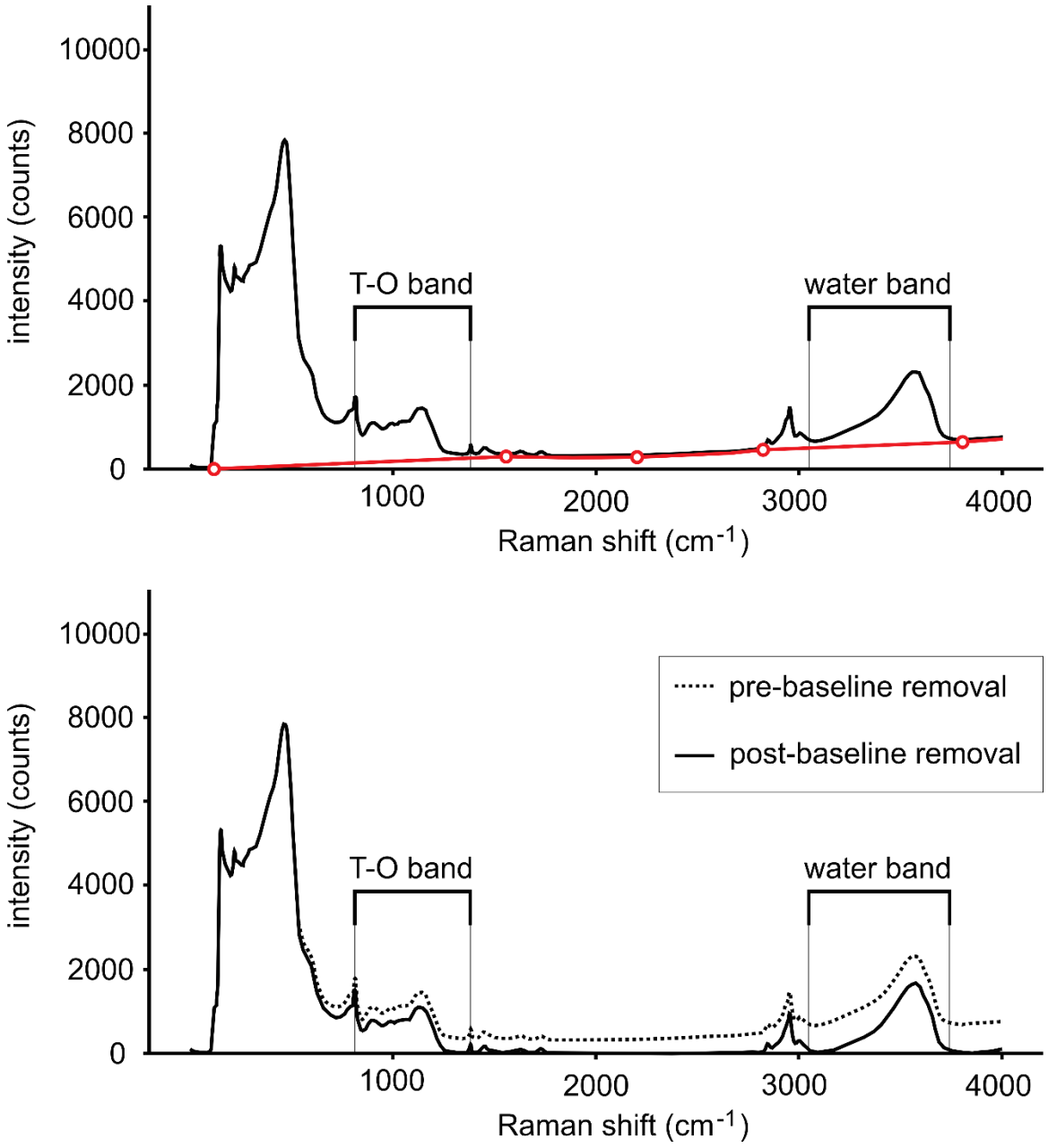

Figure 4: Baseline removal of sample 1-8-6 B. The manual baseline subtraction tool in Fityk was used to extrapolate the baseline from the flat spectral region between 1,250–1,850 cm-^{1}.

3.3.2. Quality control: Baseline removal

Zajacz et al., (2005) notes that even small variations in the baseline correction result in drastic changes to the deconvolution of the spectra, and ultimately the derived water content. In order to test the reproducibility of this method, baselines were drawn multiple times for the same spectra of samples 1-8-6 B, T 1-5-6, and 1-14-9 A (representing our full compositional suite of glasses). These duplicates underwent further spectral treatment (described henceforth), and deconvolution to quantify the effects of baseline variability on derived water content.

3.3.3 Frequency-temperature correction

It is important to note a discrepancy in the efficiency of Raman scattering as a function of the Raman shift. As the Raman shift increases, the peak intensity produced by Raman-active species will sharply decrease (Zajacz 2005). As such, Raman species that appear at high wavenumbers will generate disproportionally lower signals than species at lower wavenumbers. The heights and areas of these high-wavenumber peaks are thus not representative of the true abundance of those species. This is especially deleterious to our calibration, as the true area of the water band (which appears relatively high along the Raman shift) is needed to derive the abundance of H_2O. Without correction, this disproportionately lower water band area would report a lower water content than the true water content of the sample. As such, application of the Long correction is needed to derive a true abundance of these high Raman-shift species. This correction will amplify Raman peaks at higher wavenumbers, while maintaining the intensity of the low-wavenumber peaks proportional to their species abundance. The Long correction also allows for

comparison of spectra taken at different incident laser excitation lines, and at different temperatures (Le Losq, 2012).

$$R(v) = \frac{V_o^{3}(1-e^{[(-hcV_i)/(KT)]})\,V_i}{(V_o - V_i)}$$

Where Vo= wavenumber of the Raman laser (in this study, 532nm laser = 18796.99 cm–1), h= Planck's Constant, c= speed of light, k= Boltzmann's constant, T= sample temperature in °K, e= Euler's number, and Vi= measured wavenumber in cm^{-1}. The effects of the Frequency-temperature correction are illustrated in *Figure 5*. The spectral intensity of the high wavenumber species (i.e. the water band and surrounding peaks) becomes much higher than the low wavenumber species. Although the relative intensity of both regions is reduced, the spectra are now representative of the true abundance of these species.

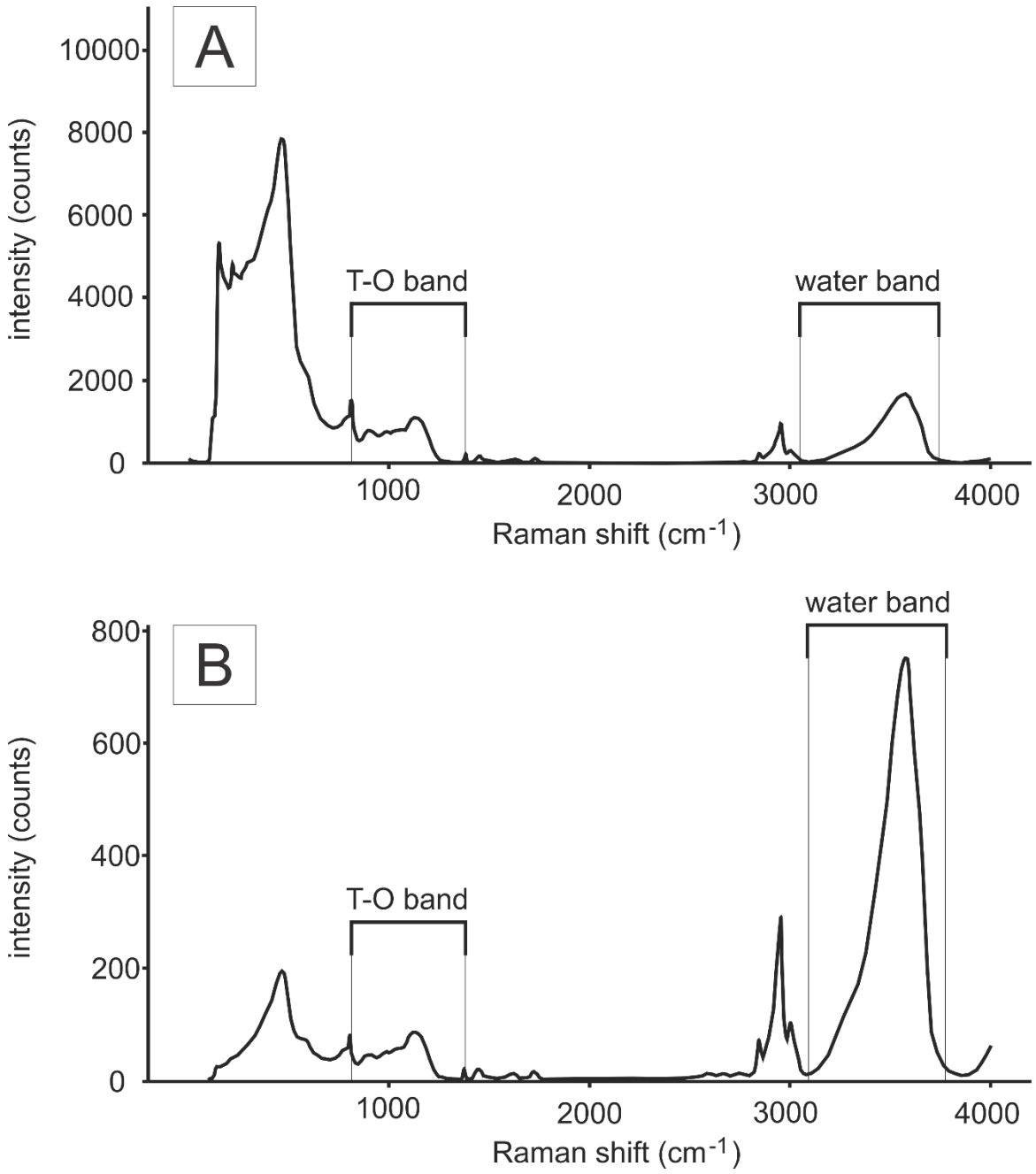

Figure 5: Spectra 1-8-6 B before (A) and after (B) application of the frequency-temperature correction. Note that intensity (counts) becomes drastically reduced after the application of this correction.

3.4 Deconvolution

Deconvolution involves finding the peak areas of the spectra, which will ultimately be used to derive the total water content of the sample. As noted by Thomas (2000), Le Losq (2012), and others, there is a strong relationship between the water content of a glass and the area ratio between the water band and the T-O band at either 470–570 cm^{-1} or 850-1250cm^{-1}. The T-O area itself has no relation to the actual water content of the glass, but is used to calibrate the water band as a semi-consistent peak feature that is present in all (hydrous) silicate glasses. First, we must decide which region of the T-O band (470–570 cm^{-1} or 850-1250cm^{-1}) is most appropriate to normalize our water band. This is dependant on the compositional suite of glasses to be analyzed.

Studies by Thomas (2000) and Chabiron et al. (2004) successfully determined water content by normalizing the area of the water band to the T-O region at 470–570 cm^{-1}. However, these studies are limited to a narrow compositional range of rhyolitic glasses. As noted by Zajacz et al. (2005), application of this method to glasses of intermediate to mafic composition proved difficult and led to inconsistent results. This was likely due to a large variability in the area of the 470-570 cm^{-1} region as a function of glass composition. To compensate, Zajacz et al. (2005) employed a much broader T-O region (from ~850-1250cm^{-1}) to calibrate the water band area. By broadening this spectral window, they were able to better account for composition-dependant changes in the T-O area, instead of relying on the area of a single peak.

For an even broader suite of hydrous glasses (including rhyolitic, trachytic, and dacitic compositions), the T-O window proposed by Zajacz et al. (2005) could be expanded

further. As shown in *Figure 6*, the shape, position, and area of the T-O band changes as a function of composition, notably in the region just before 850cm^{-1}. These changes must be accounted for in the calibration of the spectra. As such, to account for compositional variations between rhyolitic, trachytic, and dacitic glasses, the T-O region proposed by Zajacz et al. (2005) has been expanded to 700-1,250 cm^{-1}.

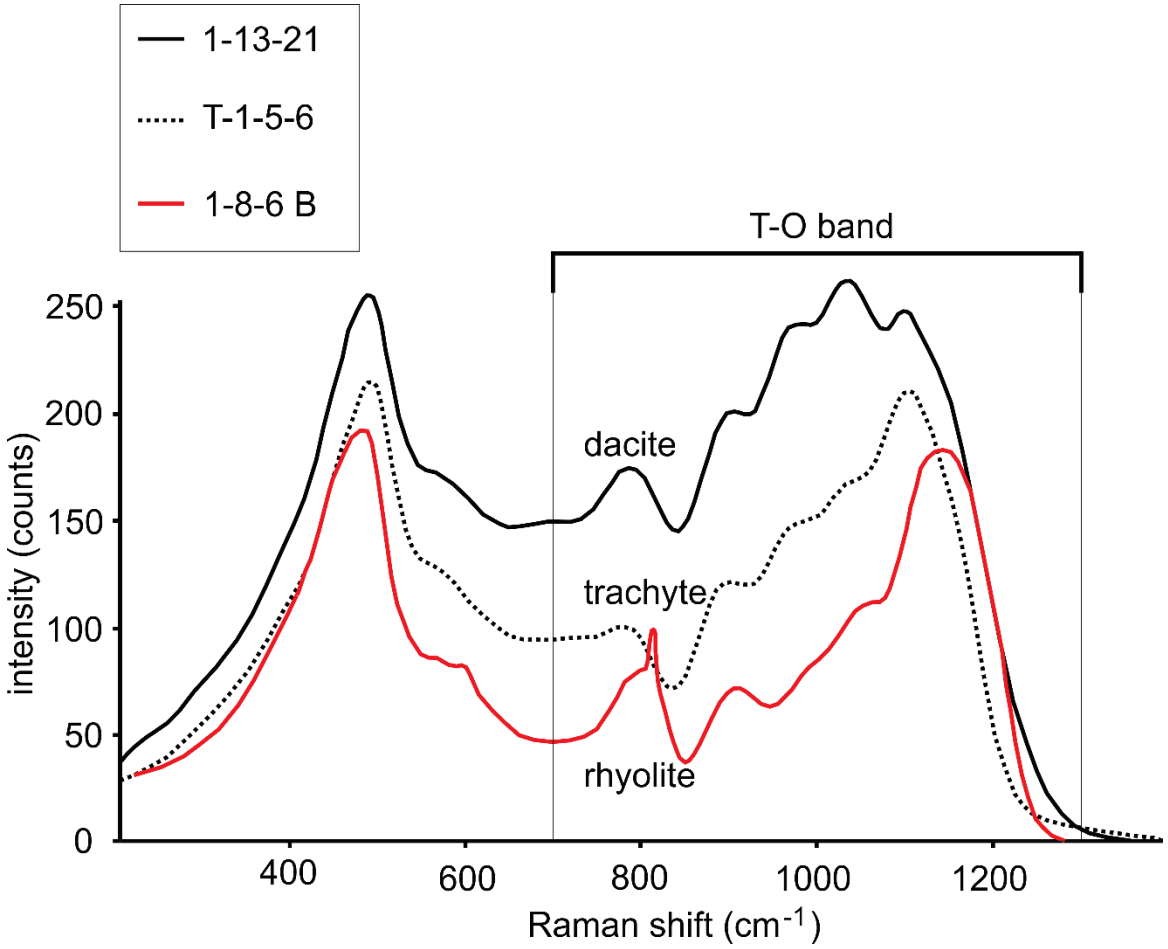

Figure 6: Change in shape/position of the T-O region as a function of composition. Spectra shown are 1-13-21 (dacitic, top), T-1-5-6 (trachytic, middle), and 1-8-6 B (rhyolitic, bottom).

Using Fityk software, the T-O band and water band spectral regions underwent deconvolution. Fityk has several curve-fitting functions that can be used to evaluate peak areas, such as Gaussian, Lorentzian, Voigt, Pearson VII, EMG, and Doniach-Sunjic (Wojdyr, 2010). Although any of these functions could be used to quantify peak areas, the Gaussian function, which produces a symmetric bell curve, diminished residual values to the greatest extent. As such, the water band and T-O region of the spectra were fitted using Gaussian functions, with each region taking 4-10 Gaussian peaks to diminish residual effects (See *Figure 7*). Once drawn, the sum of all Gaussian functions were taken for each region to derive peak areas for the T-O and water band.

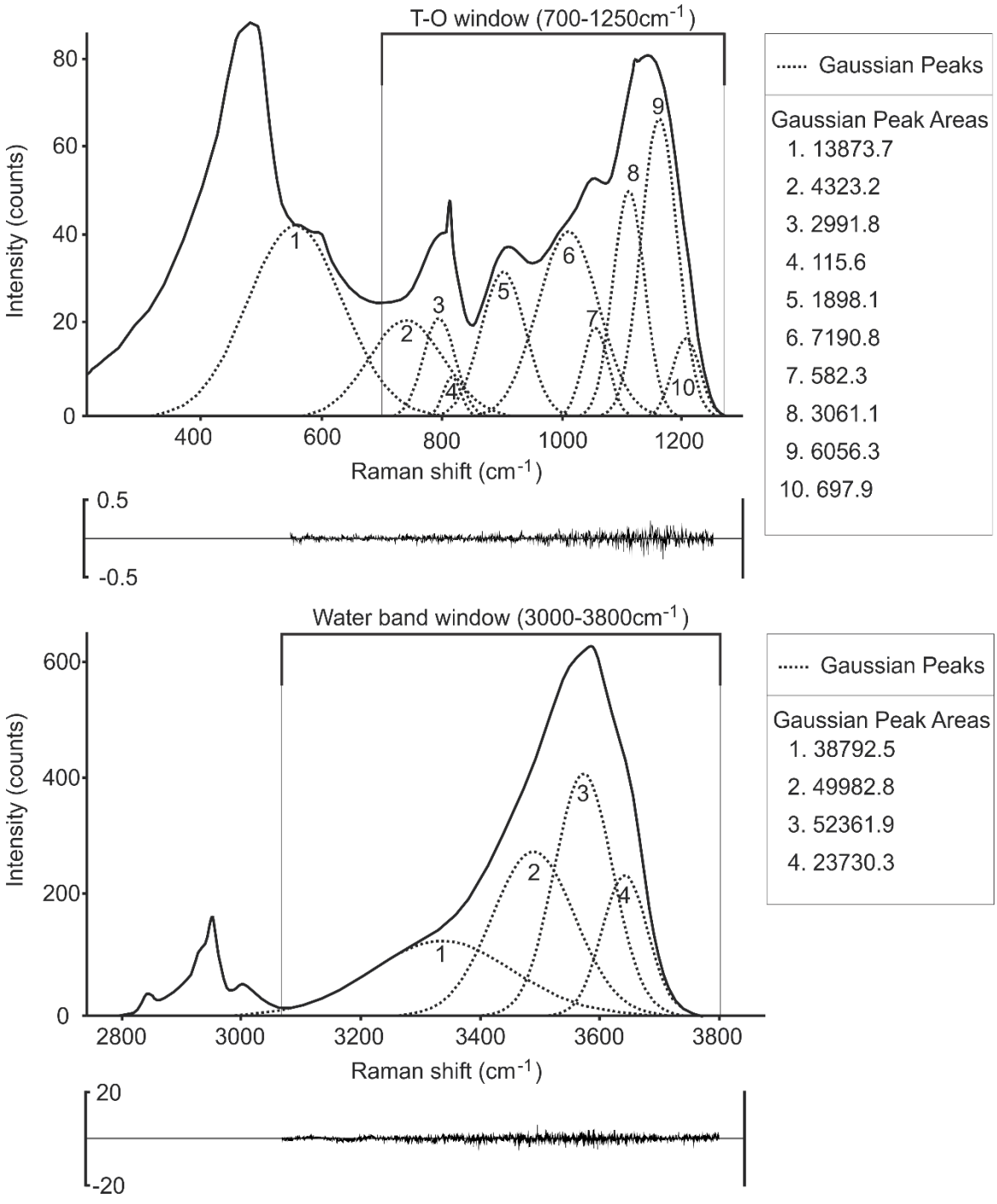

Figure 7: Deconvolution of T-O and Water band regions for sample 1-8-6 B. The residual is shown below each spectra

In some instances, the Gaussian peaks would encroach into areas beyond their intended spectral range. This was most prevalent around the 700cm^{-1} area, as shown in *Figure 7* with peaks 1 and 2. Fityk cannot measure partial peak areas, and as such, the true area for the 700-1250cm^{-1} band had to be derived manually. This was done using a pixel-counting program called Image J (National Institutes of Health), in which the sum of all peaks below the 700cm^{-1} mark were subtracted from the total peak area. This produced true area of the 700-1250cm^{-1} band (See *Figure 8*).

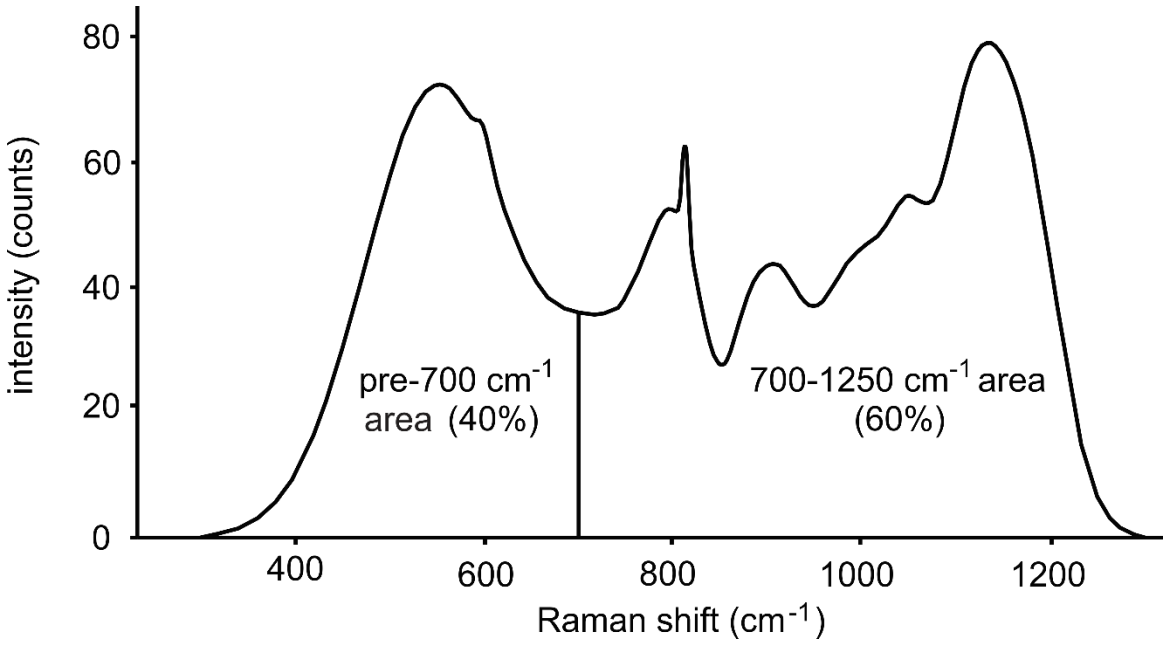

Figure 8: Partitions created in ImageJ to remove the pre-700cm^{-1} area from the total peak area. In this example, the pre-700cm^{-1} area counted 151978 out of 391708 total pixels, which represents roughly 40% of the total area. As such, 40% of the total area (i.e., the sum of all Gaussian peaks) was removed to derive the true area for the 700-1250cm^{-1} band

3.5 Water equation

The following equation, derived by Zajacz et al. (2005), normalizes the water band to the T-O region while also correcting for compositional effects caused by the T-O band.

$$\text{Water}_{\text{tot}} = 0.211 \frac{\text{Water band area}}{\text{T-O band area}} \left[\frac{1130\text{-(T-O peak position)}}{95} + 0.69 \right] T_{\text{tot}} A_1$$

Where $\text{water}_{\text{tot}}$ is the total water content in wt%, "Water band area" is the sum of all Gaussian peaks between ~3000 and ~3800 cm^{-1}, "T-O band area" is the sum of all Gaussian peaks between ~700 and ~1250 cm^{-1}, "T-O" peak position is the position of the maxima of the T-O band region, T_{tot} is the total cations of the sample, and A1 is a correction factor derived for each glass composition. The correction factor adjusts the H_2O value derived from the water equation (which is first calculated without "A1") to be closer to the actual value of H_2O. It is determined by taking the quotient between calculated vs. true H_2O values for each glass and averaging. This correction factor is unique to each Raman instrument, as instrumental effects, spectrometer settings, and other factors will alter the peak areas of acquired spectra (Behrens, et al., 2006). At the end of our calibration, we found a correction factor of 2.68 for rhyolites, 2.01 for dacites, 2.79 for trachytes.

As mentioned previously, the shape and size of certain peaks within the T-O band will change as a function of composition (see *Figure 6*). In order to account for these effects, the water equation makes a linear correction based on the total number of tetrahedral cations in each sample. This theoretical consideration is based on the fact that T-O band is comprised of different T–O–T and T–O species in the glass's structure, and that the

abundance of each species is related to the total number of tetrahedral cations in the sample. Compositional changes can also manifest as a shift in T-O band position, due to different ratios of T-O and T-O-T structural species in the glass. As such, the position of each T-O band is also corrected relative to a rhyolitic standard with an NBO/T (number of non-bridging oxygen atoms divided by the number of tetrahedral sites) close to 0, which has a T-O peak maxima at 1130cm^{-1} (Zajacz et al., 2005)

3.6 Raman analysis of fluorescing inclusions

A major drawback of Raman spectroscopy (in the visible light range) is fluorescence, which creates background noise that can obscure Raman peaks, as shown in *Figure 9*. Fluorescence occurs because the Raman scattering effect is relatively weak, with only 1 in 104 photons from the incident laser light interacting successfully with a Raman-active species. Fluorescence, in contrast, is much stronger than the Raman effect, and forms through similar molecular interactions. As such, the energy required to produce excitation in a Raman active species is much less than that required to generate fluorescence. Any minor contaminant in the sample which is fluorescent can thus produce signals (Smith, 2005). In consequence, Raman spectra can become completely overwhelmed by the fluorescence background, which is also thought to be the main contributor to the shape of the baseline shape (Le Losq, 2012).

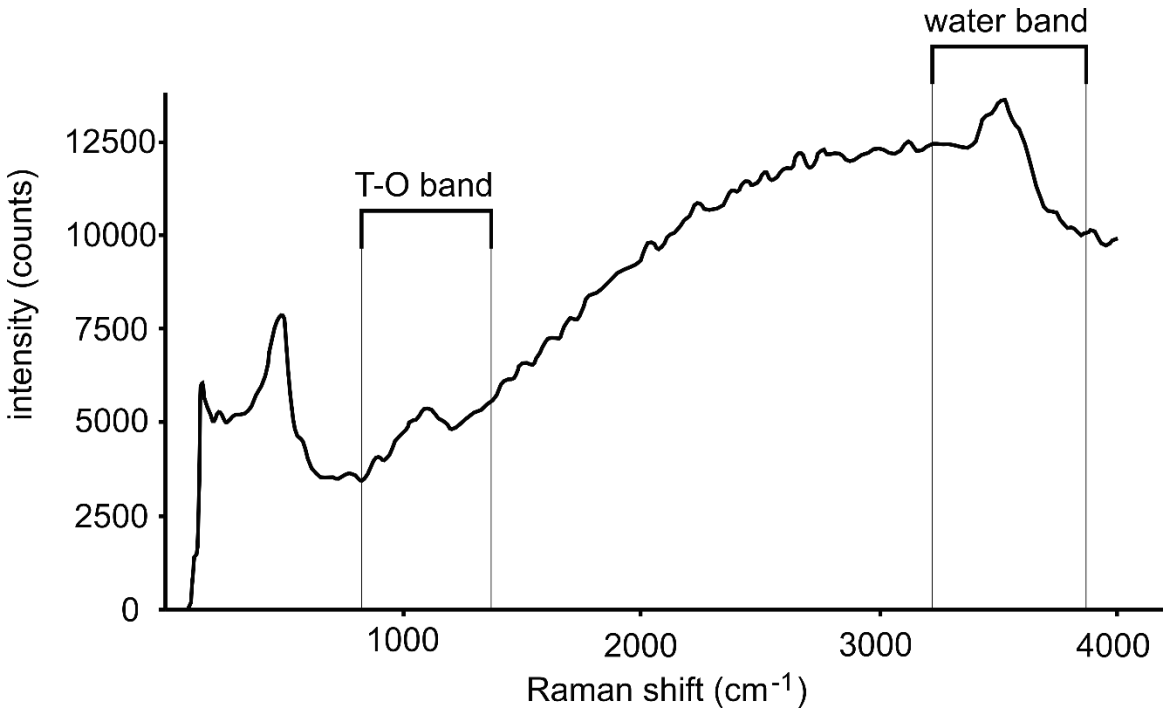

Figure 9: Uncorrected spectra showing the effects of fluorescence, which causes the water band between ~3000 and ~3800 cm^{-1} to ride atop a large fluorescence peak. This can interfere with baseline correction and reduce the accuracy and reproducibility of water determination.

Ideally, samples should be physically homogeneous and transparent. Coloured and translucent samples are rapidly overheated by absorption of laser beam energy, which can result in fluorescence (Campbell et al., 1986). Other contributing sources to fluorescence include fingerprints, dissolved iron, defects in the crystal lattice, water absorption near the sample's surface, and the excitation of the embedding resin (Smith, 2005, Chabiron et al., 2004, Mercier et al., 2009, Behrens et al., 2006, and Le Losq, 2012). Seven of our samples were affected by fluorescence, including sample 1-10-15 A-C, 1-13-21, 1-15-04, T 1-4-14, and T 1-5-6. As most natural and synthetic samples are affected by this phenomenon, it is important to quantify how fluorescence effects the spectra. The following steps were taken to investigate the effect of fluorescence on water peaks, and to mitigate its effects:

i. Develop anhydrous equivalents of the synthetic glass
ii. Analyze the glasses under UV radiation

3.6.1 Anhydrous samples

From *Figure 9*, it is difficult to tell if the water band is riding atop the fluorescence peak, or if it's being partially obscured by the fluorescence in some way. In order to quantify how fluorescence affects the spectra, anhydrous analogues were made of the fluorescent glass and analyzed via Raman spectroscopy (the details of this glass synthesis are discussed in section 3.1). The resultant spectra, sans hydrous components, will be subtracted from the normal spectra thus removing the fluorescent components and leaving only the water peak behind. This spectral subtraction was carried out using the "A-B" subtraction function in LabSpec 6 (see *Figure 10* and *11*). Note that this subtraction was limited to the water band region at ~3600cm^{-1}, in order to preserve the T-O region (which is present in both the hydrous and anhydrous glasses). To do so, the anhydrous spectra was trimmed to a range

of 1500-4000 cm^{-1} before subtraction took place. The resultant "subtracted spectra" underwent spectral treatment, deconvolution, and water determination (as described in sections 3.3-3.5).

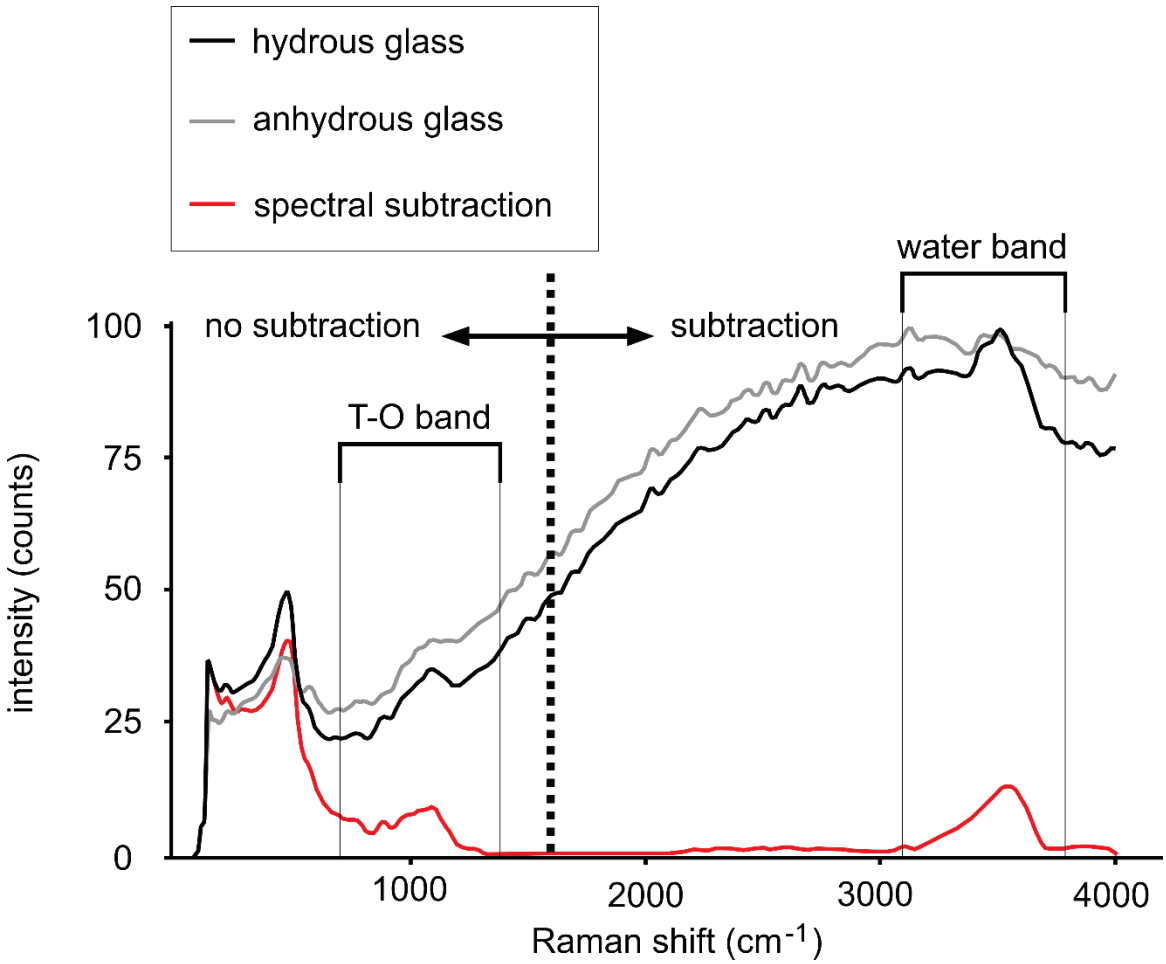

Figure 10: Hydrous and anhydrous equivalent of sample T 1-4-14. Spectra were subtracted from each other using the "subtract" function in LabSpec 6, giving the resultant spectra shown in red. Note that this subtraction was limited to the water band region of the spectra, in order to preserve the T-O band region, which shows up in both the hydrous and anhydrous glasses.

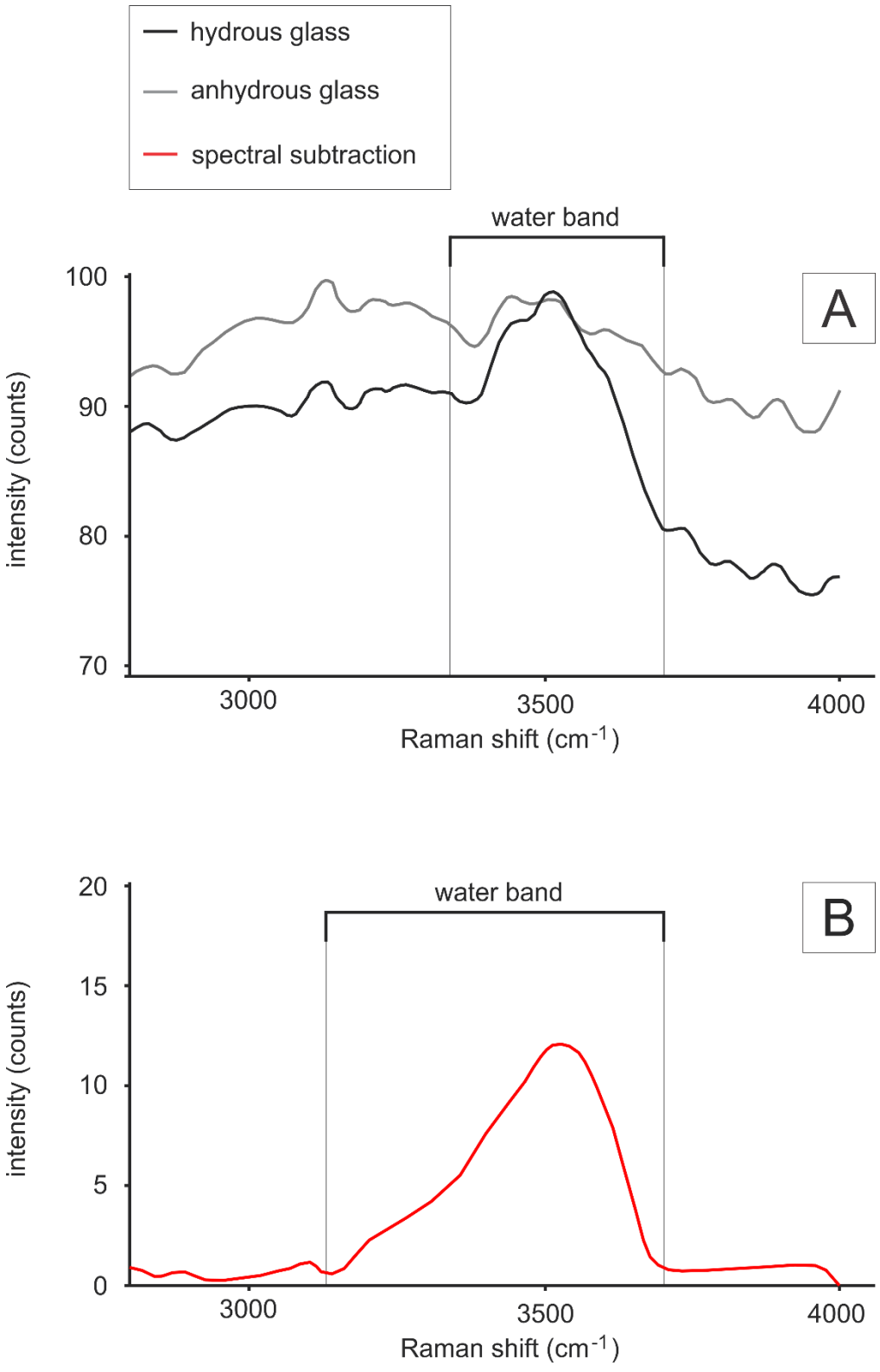

Figure 11: Highlight of the T-O region for (A) the hydrous and anhydrous equivalents of sample T 1-4-14 and (B) the subtracted spectra. Note how all fluorescent components are removed from the subtracted spectra.

3.6.2 UV spectroscopy

A proven method to minimize fluorescence is to use a Raman laser with a lower wavelength, such as in the UV region (244 nm). As noted by Millen et al. (1999) and Severs et al. (2007) fluorescence can be reduced or completely mitigated by recording spectra at this very short wavelength. In most UV-excited systems, fluorescent energy will be dissipated into the material, due to interactions with electronically excited states. Even if some fluorescence is radiated by the material, the emitted wavelength will be beyond the region used for Raman detection (Smith, 2005).

In order to quantify the true effects of fluorescence on the spectra, the fluorescent samples 1-10-15 A, T 1-4-13, and 1-15-4 were analyzed using UV Raman spectroscopy. Samples were sent to the HORIBA Scientific labs in Edison, New Jersey and were analyzed using a near-UV 405nm Raman laser. The resultant peaks were then analyzed for water content (following the procedure from 3.3-3.5).

4.0 Results and discussion

4.1 Raman parameters

A variety of settings were adjusted iteratively to produce the highest-resolution Raman spectra. These include the confocal hole size, grating, laser power, number of accumulations, and acquisition time. A high spectral resolution is important, as it will reveal subtle details of the spectra that might not be apparent at lower resolution (Adar, 2013). The effects of these settings on acquired spectra are outlined in *Figures 12-16*, which shows that a high hole size, power, and acquisition time appear to increase spectral resolution. The number of accumulations also positively affects the resolution, but does not

make much difference beyond an accumulation of four. Grating gives a higher resolution at 600 rather than 1800 grooves/mm, but also enhances the fluorescent background of the sample, which obscures the water band at ~3600cm^{-1}.

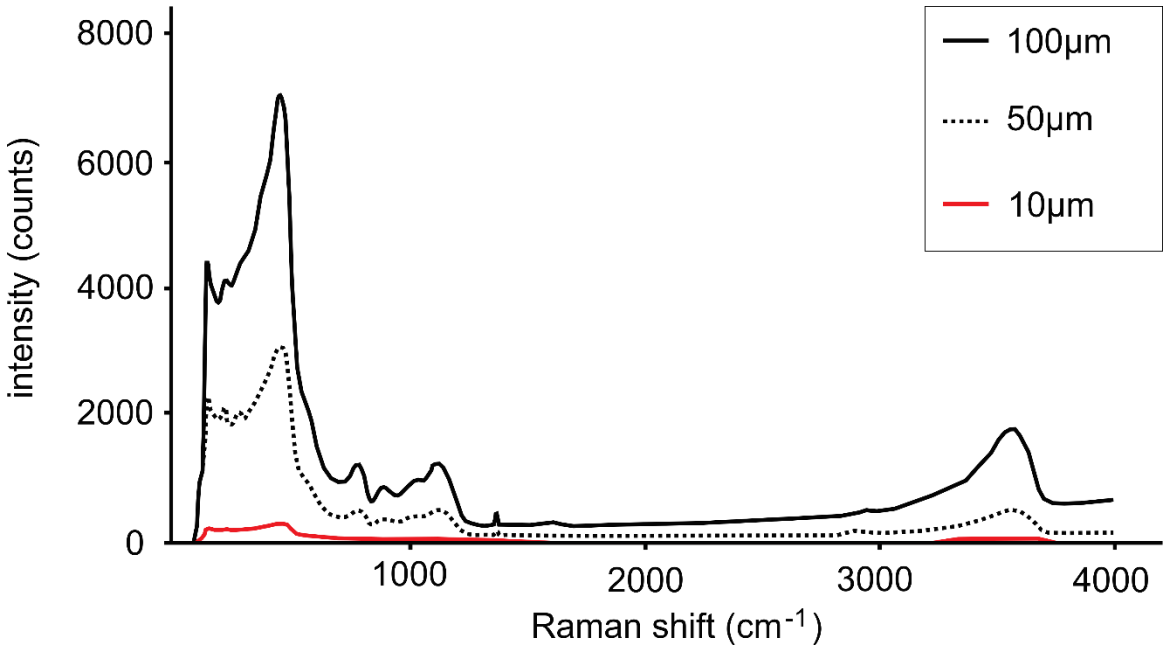

Figure 12: Effect of hole size on resolution

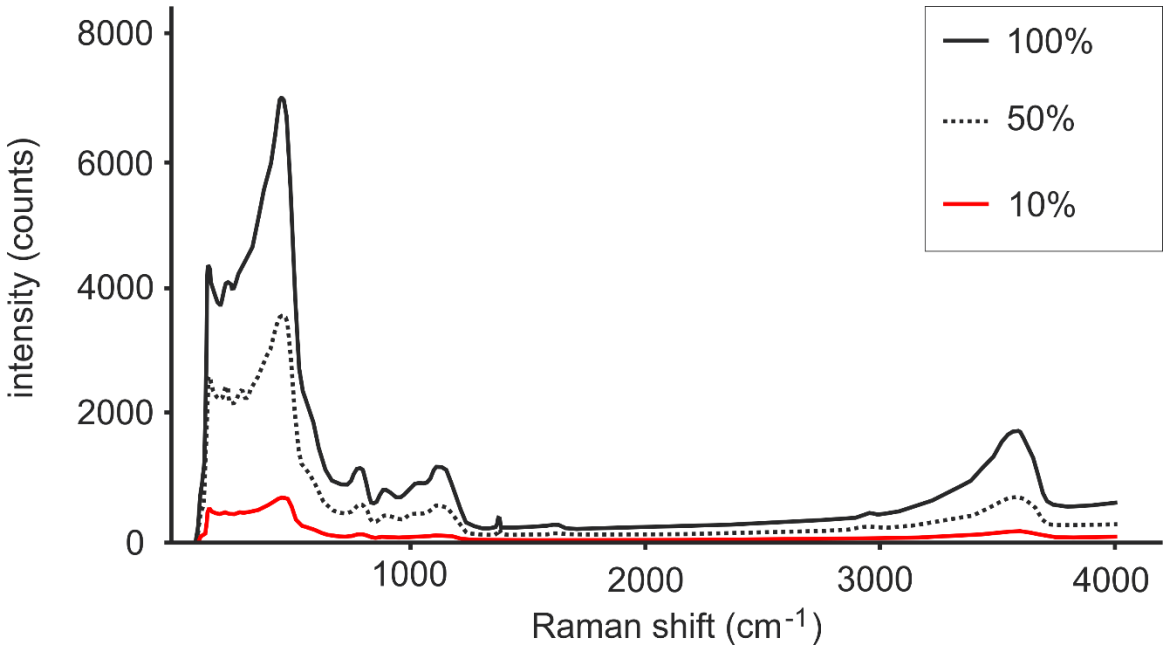

Figure 13: Effect of laser power on resolution. At 100% laser power, there is ~2.15 mW at the sample surface.

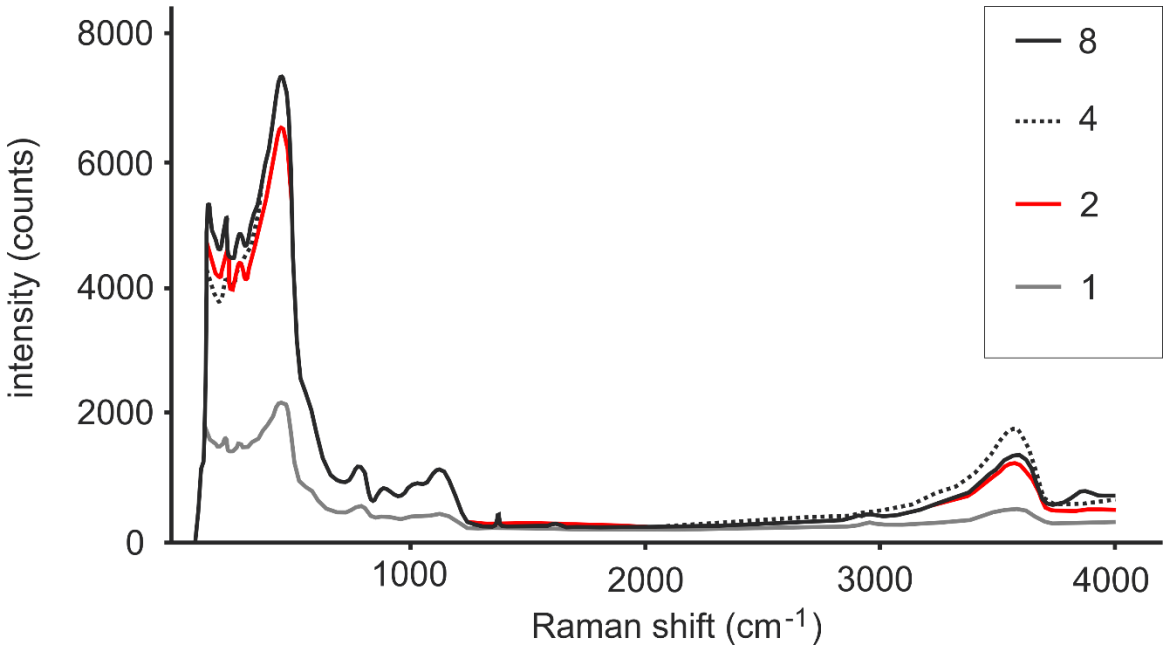

Figure 14: Effect of the number of accumulations on resolution.

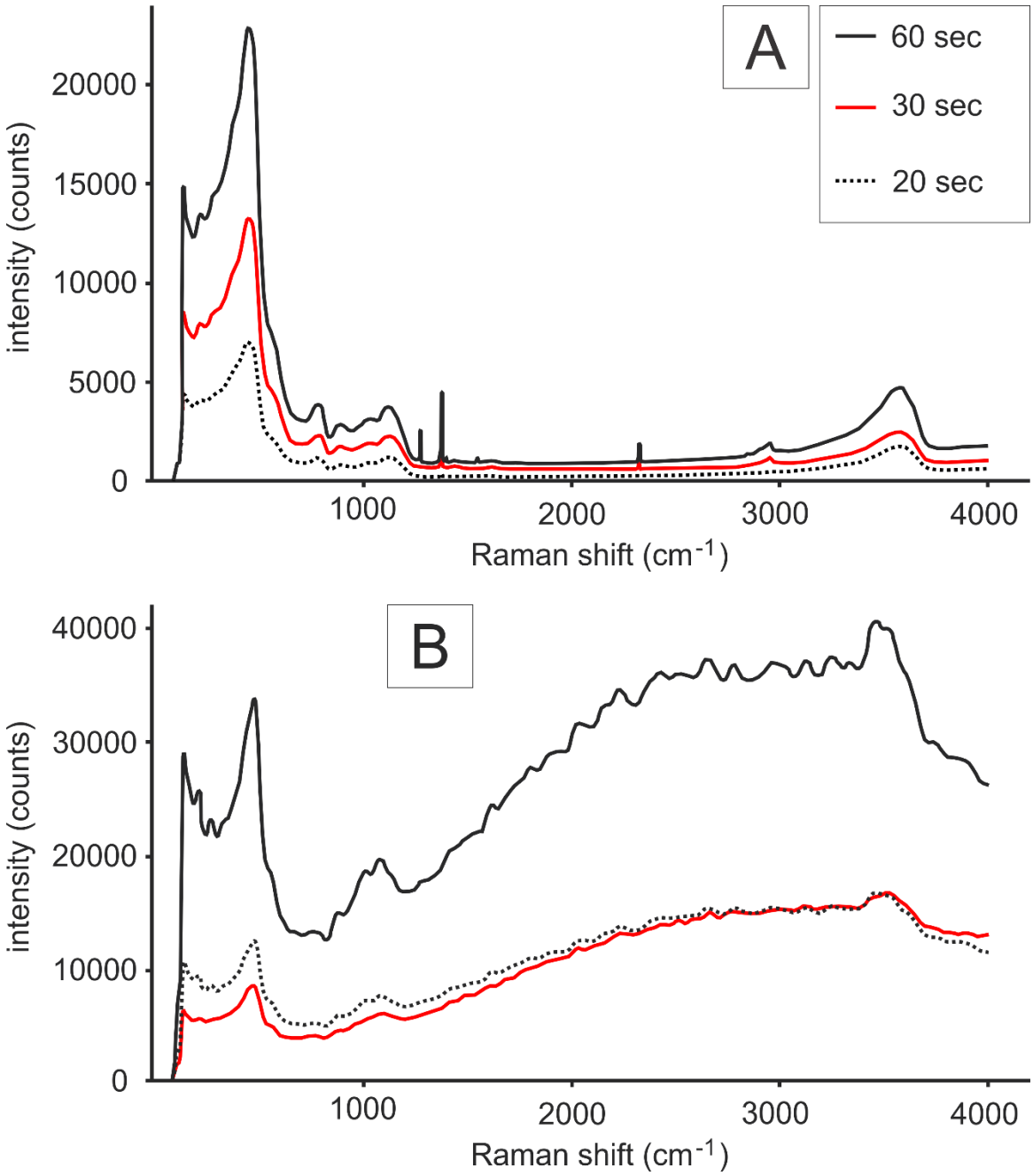

Figure 15: Effect of acquisition time on resolution for a non-fluorescent sample (A) and a fluorescent sample (B).

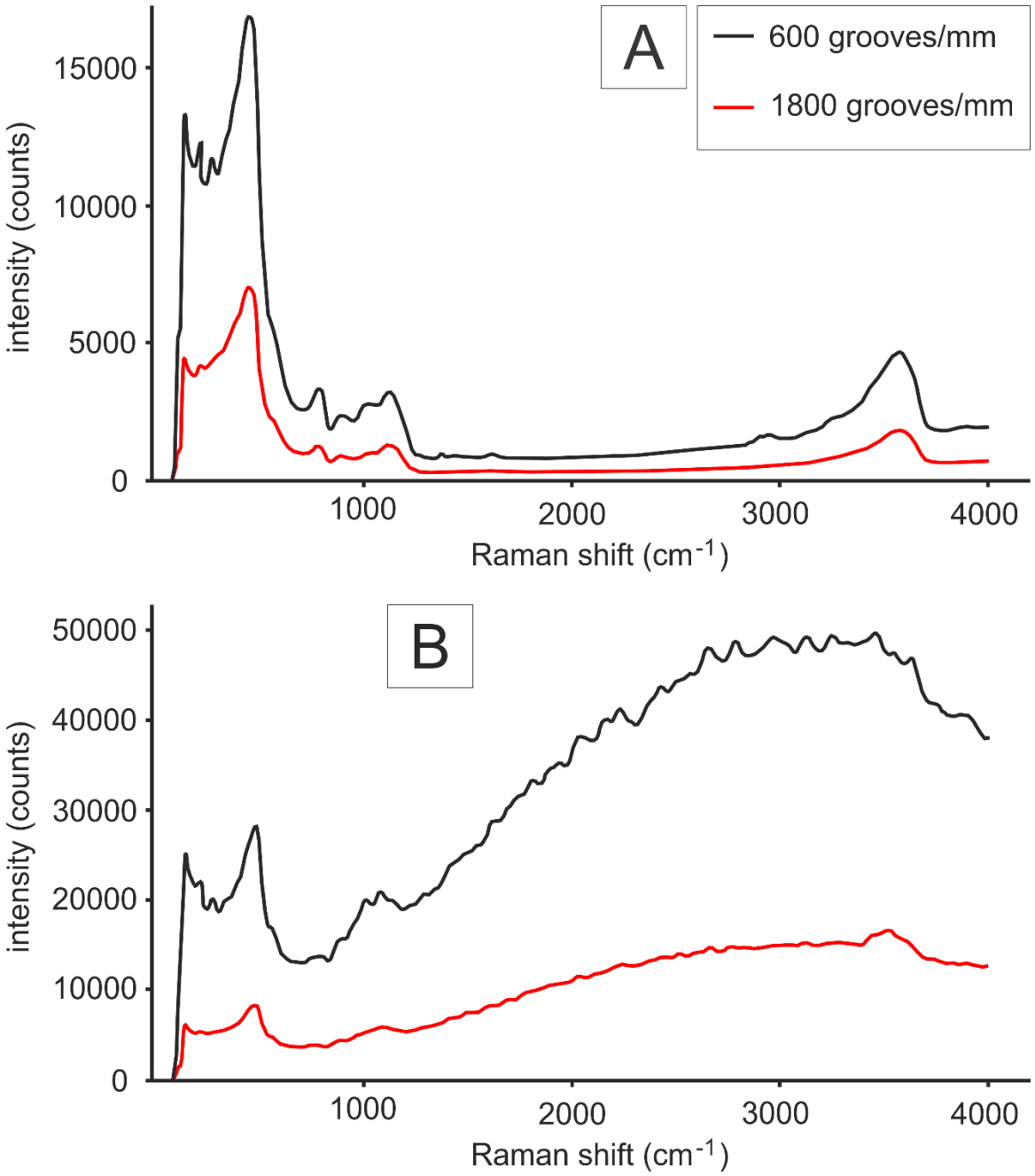

Figure 16: Effect of grating on resolution for a non-fluorescent sample (A) and a fluorescent sample (B).

4.1.1 Confocal Hole Size

Hole size has a very clear effect on spectral resolution. The Confocal hole (or aperture) controls how much of the Raman signal passes through the spectrograph and onto the detector (Wieboldt, 2010). As such, a smaller confocal hole results in a lower resolution image, while a large hole size results in a high-resolution image. Smaller aperture sizes are typically only used to analyze samples that are smaller than the beam diameter. Samples examined in this way are usually only ~1μm across (Smith, 2005). As such, the hole size for our study was set at 100μm.

4.1.2 Power

The intensity of the Raman spectra appears directly proportional to the power of the Raman laser. It should be obvious that the more energy used to excite the sample, the stronger the signal will return. As such, it is commonly recommended to use 100% laser power first when optimizing Raman parameters for spectral resolution (Wieboldt, 2010). Accordingly, the power for our study was set at 100%.

4.1.3 Accumulations

Multiple exposures of the same Raman spectra can be combined to reduce its overall signal-to-noise ratio. This is the principle behind the number of accumulations (Wieboldt, 2010). The number of accumulations appears to have a positive impact on spectral resolution, but it stops making a big difference past an Acc of 4 (See *Figure 14*). In addition, raising the accumulation number from 4 to 8 effectively doubles the time of analysis (from 15 to 30 minutes). In order to keep our analysis time-effective, the maximum number of accumulations was capped at 4.

4.1.4 Acquisition Time

Acquisition time is analogous to the exposure time on a photographic camera. Just as a longer exposure in dim light can produce a higher resolution image, a longer acquisition time can produce higher resolution spectra from weak Raman scattering (Wieboldt, 2010). There are, however, special considerations to be noted when choosing acquisition time. From *Figure 15-B*, we can see that an increased acquisition time enhances the fluorescent background of the sample. This may alter the area of the Raman peaks, which will ultimately effect the water content determination. Damage is also a concern, as samples with a dark colouration or with an absorption band close to the excitation wavelength may become burned by the laser (Wieboldt, 2010). Damage can occur in a large volume of glass over a short time, and can affect the Raman scattering of the sample (Smith, 2005). Additionally, an acquisition time past 20 seconds caused saturation of the Raman detector for certain samples. As such, to get consistent readings for calibration, the acquisition time was lowered to 20 sec.

4.1.5 Grooves

From *Figure 16*, it appears that the lower the groove density of the grating, the higher the spectral resolution. Ideally, peak intensity/resolution should be maximized while keeping the effects of fluorescence to a minimum. The fluorescent background is greatly enhanced at 600 grooves/mm for our fluorescent samples, effectively obscuring the water band at ~3600cm^{-1}. As such, the 1800 groove setting was used in our Raman analysis to help combat the effects of fluorescence.

To summarize, the analysis of silicate glass is best performed with a 100-micron confocal hole diameter, 1800 grooves/nm grating, four accumulations, twenty second acquisition time, and 100% laser power. This produced a final spectral resolution of $\pm 0.45 cm^{-1}$.

4.2 Quality control (reproducibility assessment)

It is important to quantify the largest source of error in our water determination. As mentioned previously, Zajacz et al. (2005) found that uncertainties in the baseline correction lead to large uncertainties in deconvolution, and ultimately the water determination of the sample. However, the effects of heterogeneity of the glass may also alter the final water content, and must also be explored as a possible source of error. As such, the baseline uncertainty was tested by applying the baseline correction to the same spectra over a large number of trials. This was done on a representative suite of glasses, to include our full compositional range of rhyolitic, trachytic, and dacitic samples. To test the effects of heterogeneity, the same procedure was followed using different spectra for each glass, which were collected in different areas of the same chip. *Tables 4* and *5* show the peak areas, H_2O content, and error derived for each trial, with error calculated as a standard deviation for each glass type (with 18 repeat analyses per glass). *Figures 17* and *18* illustrate the variation in final derived H_2O content caused by these effects, which is lowest for the rhyolitic and dacitic glasses, and high for the trachytic glasses.

From *Tables 4* and *5*, it appears that the "heterogeneity+baseline" test produces a larger error than the pure "baseline" test (± 0.52, 0.48, and 0.96 vs. 0.17, 0.36, and 0.72 wt% H_2O error for rhyolitic, dacitic, and trachityc glasses respectively). If glass heterogeneity does not contribute to the overall error in the experiment, we would not expect the error

associated with this trial to be much different than the “pure” baseline trial. However, the error associated with the heterogeneity+baseline test is significantly larger than the baseline test, which suggests that compositional differences within each sample will contribute to the overall water determination. As such, it is recommended for future studies that multiple spectra of each glass be taken in different regions of the sample, to account for the error associated with both baseline removal and sample heterogeneity.

Table 4: Baseline error calculations (H_2O values in wt%)

Sample #	1-8-6 B																	
T-O area[1]	1384	1392	1414	1337	1368	1406	1372	1296	1399	1394	1387	1356	1339	1325	1493	1435	1422	1451
Water area[2]	34341	30424	30109	29892	30715	30166	30900	30041	31821	28878	30629	30360	30091	33991	33229	31779	30990	31500
Calc H_2O[3]	4.68	4.12	4.01	4.22	4.23	4.05	4.25	4.37	4.29	3.91	4.16	4.22	4.24	4.84	4.20	4.18	4.11	4.09
True H_2O[4]	2.68	2.68	2.68	2.68	2.68	2.68	2.68	2.68	2.68	2.68	2.68	2.68	2.68	2.68	2.68	2.68	2.68	2.68
Corrected H_2O[5]	3.78	3.33	3.24	3.41	3.42	3.27	3.43	3.53	3.47	3.16	3.36	3.41	3.42	3.91	3.39	3.37	3.32	3.31
Variation[6]	**0.17**																	
Sample #	1-14-9 A																	
T-O area[1]	1667	1744	1821	1656	1747	1700	1668	1686	1666	1779	1813	1719	1582	1756	1633	1742	1767	1632
Water area[2]	41154	42700	43856	42926	43431	38778	38879	42024	41175	42875	41592	38734	40993	40212	42520	39004	40111	42474
Calc H_2O[3]	11.90	11.80	11.60	12.49	11.98	10.99	11.23	12.01	11.91	11.61	11.05	10.86	12.48	11.03	12.55	10.79	10.94	12.54
True H_2O[4]	5.44	5.44	5.44	5.44	5.44	5.44	5.44	5.44	5.44	5.44	5.44	5.44	5.44	5.44	5.44	5.44	5.44	5.44
Corrected H_2O[5]	7.10	7.04	6.93	7.45	7.15	6.56	6.70	7.17	7.11	6.93	6.60	6.48	7.45	6.59	7.49	6.44	6.53	7.48
Variation[6]	**0.36**																	
Sample #	T 1-5-6																	
T-O area[1]	1166	1281	1122	1268	1409	1190	1203	1265	1217	1410	1221	1217	1186	1301	1186	1163	1298	1353
Water area[2]	31643	37710	37557	38867	37391	39422	37747	37558	39595	34994	35676	44054	41804	34512	39595	37542	40107	37467
Calc H_2O[3]	7.59	8.23	9.36	8.57	7.42	9.26	8.77	8.30	9.09	6.94	8.17	10.12	9.86	7.42	9.33	9.02	8.64	7.74
True H_2O[4]	5.34	5.34	5.34	5.34	5.34	5.34	5.34	5.34	5.34	5.34	5.34	5.34	5.34	5.34	5.34	5.34	5.34	5.34
Corrected H_2O[5]	6.30	6.83	7.77	7.11	6.16	7.69	7.28	6.89	7.55	5.76	6.78	8.40	8.18	6.16	7.75	7.49	7.17	6.43
Variation[6]	**0.72**																	

[1]the sum of all Gaussian peaks between ~700 and ~1250 cm^{-1}

[2]the sum of all Gaussian peaks between ~3000 and ~3800 cm^{-1}

[3]the wt% H_2O content for each sample calculated using the water equation

[4]the actual wt% H_2O of the sample calculated via FTIR spectroscopy

[5]the wt% H_2O content for each sample after application of the correction factor

[6] the difference in calculated wt%H_2O values between each repeat analysis of the spectra within 1 standard deviation of the mean

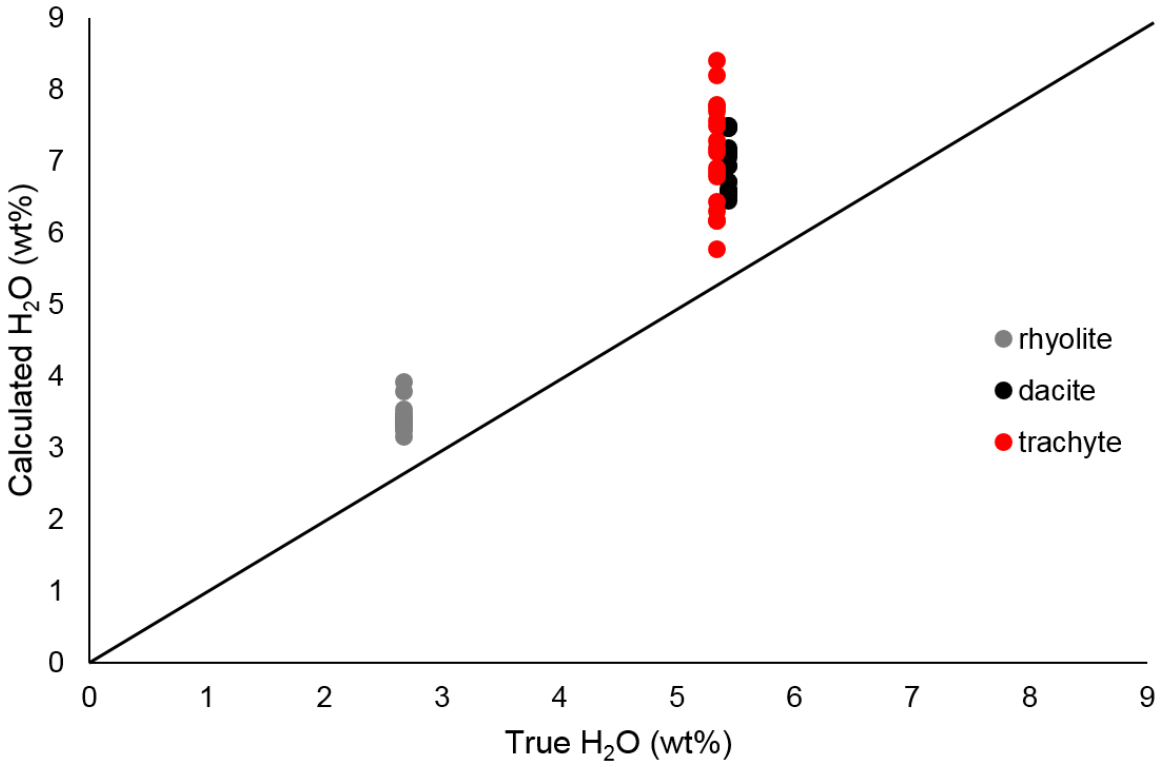

Figure 17: Variation in calculated H_2O content caused by changes in the baseline correction of the spectra. Each dot represents the final H_2O content derived from a repeat analysis using the same spectra with a different baseline correction. The error for each glass within 1 standard deviation of the mean is ± 0.17wt% for the rhyolite, 0.35wt% for the dacite, and 0.72wt% for the trachyte.

Table 5: Glass homogeneity plus baseline error calculations (H_2O values in wt%)

Sample #	1-8-6 B																	
T-O area[1]	1368	992	940	1245	1846	1225	1308	1399	1173	1357	1362	1376	1339	1476	1378	1465	1552	1429
Water area[2]	35144	32453	28363	32085	50643	33000	39390	32414	34614	32611	30860	35957	32962	31379	32127	28714	33391	32457
Calc H_2O[3]	4.84	6.17	5.69	4.86	5.17	5.08	5.68	4.37	5.56	4.53	4.27	4.93	4.64	4.01	4.40	3.69	4.06	4.28
True H_2O[4]	2.68	2.68	2.68	2.68	2.68	2.68	2.68	2.68	2.68	2.68	2.68	2.68	2.68	2.68	2.68	2.68	2.68	2.68
Corrected H_2O[5]	3.91	4.98	4.60	3.93	4.18	4.10	4.50	3.53	4.49	3.66	3.45	3.98	3.80	3.24	3.55	2.99	3.28	3.46
Variation[6]	**0.52**																	
Sample #	1-14-9 A																	
T-O area[1]	1657	1727	1928	1798	1845	1781	1429	1701	1874	1822	1966	1770	1571	1874	1865	1858	1875	1950
Water area[2]	43837	43755	42164	39979	44807	39447	37873	44071	42058	44883	42290	40995	42355	44018	42456	46211	44199	44703
Calc H_2O[3]	12.75	12.21	10.54	10.72	11.70	10.67	12.77	12.49	10.81	11.87	10.36	11.16	12.99	11.32	10.97	11.98	11.36	11.05
True H_2O[4]	5.44	5.44	5.44	5.44	5.44	5.44	5.44	5.44	5.44	5.44	5.44	5.44	5.44	5.44	5.44	5.44	5.44	5.44
Corrected H_2O[5]	7.61	7.29	6.29	6.40	6.99	6.37	7.62	7.40	6.46	7.09	6.19	6.66	7.76	6.76	6.55	7.15	6.78	6.59
Variation[6]	**0.48**																	
Sample #	T 1-5-6																	
T-O area[1]	1681	1275	1284	1527	2060	2338	2357	2159	2502	2203	2006	2311	2227	2378	2230	789	2177	2599
Water area[2]	42948	38244	32340	41210	52174	58011	60843	54018	76805	67102	59948	66114	53786	61909	70634	26156	54926	35511
Calc H_2O[3]	7.14	8.39	7.04	7.55	7.08	6.94	7.22	7.00	8.58	8.52	8.36	8.00	6.75	7.28	8.86	9.27	7.05	3.82
True H_2O[4]	5.34	5.34	5.34	5.34	5.34	5.34	5.34	5.34	5.34	5.34	5.34	5.34	5.34	5.34	5.34	5.34	5.34	5.34
Corrected H_2O[5]	5.93	6.96	5.85	6.26	5.88	5.76	5.99	5.81	7.13	7.07	6.94	6.64	5.61	6.04	7.35	7.70	5.86	3.20
Variation[6]	**0.96**																	

[1]the sum of all Gaussian peaks between ~700 and ~1250 cm^{-1}

[2]the sum of all Gaussian peaks between ~3000 and ~3800 cm^{-1}

[3]the wt% H_2O content for each sample calculated using the water equation

[4]the actual wt% H_2O of the sample calculated via FTIR spectroscopy

[5]the wt% H_2O content for each sample after application of the correction factor

[6] the difference in calculated wt%H_2O values between each repeat analysis of the glass within 1 standard deviation of the mean

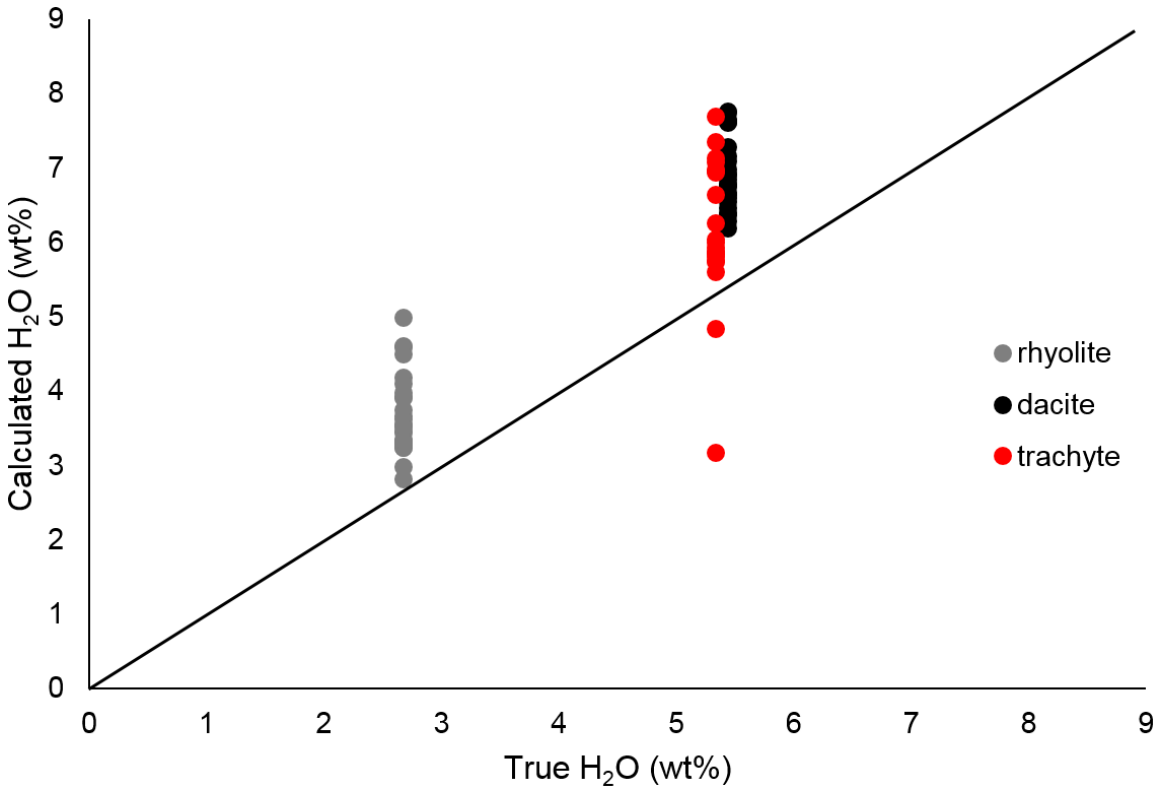

Figure 18: Variation in calculated H_2O content caused by sample heterogeneity and variations in the baseline correction of the spectra. Each dot represents the final H_2O content derived from a repeat analysis using different spectra taken from different areas of the glass, plus a different baseline correction. The error for each glass within 1 standard deviation of the mean is ± 0.52wt% for the rhyolite, 0.48wt% for the dacite, and 0.96wt% for the trachyte.

4.3 Water determination

The results of our water determination for our suite of rhyolitic, dacitic, and trachytic glasses are shown in *Figure 19* and *Table 6*. The maximum error associated with our determination is 1.29 wt% H_2O for rhyolites, 2.18 wt% H_2O for dacites, and 1.08 wt% H_2O for trachytes. The average error between all values is 0.85 wt% H_2O. Errors were calculated by taking the difference between calculated vs. true H_2O values for all glasses (See *Table 7*). The error associated with these values are in keeping with similar studies by Zajacz et al. (2005) and Di Muro et al. (2006). Uncertainties for our values are based off the 1 sigma deviation of error associated with sample heterogeneity and variation in the baseline correction of the spectra (See *Section 4.2*). This resulted in a ± 0.52 wt% H_2O uncertainty for the rhyolites, 0.48 wt% H_2O uncertainty for the dacites, and 0.96 wt% H_2O uncertainty for the trachytes.

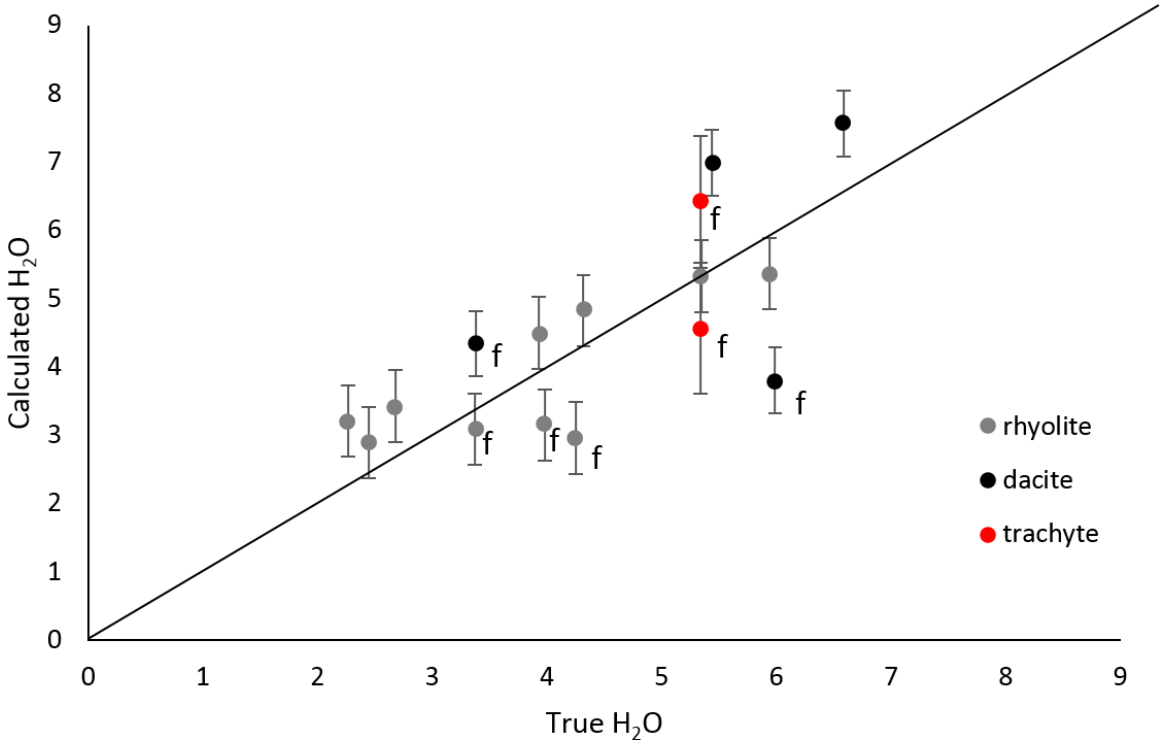

Figure 19: Calibration line for silicate glasses. "f" subscript denotes fluorescence problem with sample. Error bar values are based on the 1 sigma uncertainty derived from the error associated with glass heterogeneity and baseline variability.

Table 6: Water equation parameters (H_2O shown in wt%)

Sample #	T-O pos.[1]	T-O area[2]	Water area[3]	area StDev[4]	Ttot (FeO)[5]	T tot (Fe_2O_3)[6]	Calc H_2O[7]	True H_2O[8]	Correction Factor[9]	Corrected H_2O[10]
1-8-6 B	1139	29141	197739	1.50	1.50	1.50	1.28	2.68	2.68	3.43
1-9-10 A	1139	26479	294147	5.63	1.44	1.44	2.00	5.94	2.68	5.37
1-9-10 B	1139	25623	249485	5.63	1.47	1.47	1.80	4.32	2.68	4.83
1-10-1 A	1139	23748	149535	5.63	1.51	1.51	1.20	2.27	2.68	3.21
1-10-1 B	1139	26801	152301	5.63	1.51	1.51	1.08	2.45	2.68	2.89
1-10-2 A	1139	27357	245946	5.63	1.49	1.49	1.68	3.93	2.68	4.50
1-10-2 B	1139	29931	316569	5.63	1.50	1.50	1.99	5.35	2.68	5.33
1-10-15 A	1139	40752	243501	5.63	1.46	1.47	1.11	4.25	2.68	2.96
1-10-15 B	1139	27945	177544	5.63	1.46	1.48	1.18	3.98	2.68	3.15
1-10-15 C	1139	28757	179582	5.63	1.46	1.47	1.15	3.37	2.68	3.09
1-13-10	1032	45710	167976	3.34	1.38	1.42	1.90	5.99	2.01	3.81
1-13-21	1032	54113	402313	1.43	1.40	1.43	3.77	6.59	2.01	7.57
1-14-9 A	1035	33912	244771	1.39	1.35	1.39	3.48	5.44	2.01	6.99
1-15-4	1032	43440	175764	3.34	1.43	1.47	2.16	3.38	2.01	4.34
T 1-4-13	1095	29784	156783	11.80	1.38	1.40	1.64	5.34	2.79	4.57
T 1-5-6	1103	40749	335438	1.37	5.90	1.37	2.30	5.34	2.79	6.42

[1]the position of the maxima of the T-O band region

[2]the sum of all Gaussian peaks between ~700 and ~1250 cm^{-1}

[3]the sum of all Gaussian peaks between ~3000 and ~3800 cm^{-1}

[4]the standard deviation of the ratio between the T-O band and the Water band

[5]the total number of T-site cations in the sample using ferrous Fe in the determination

[6] the total number of T-site cations in the sample using ferric Fe in the determination

[7]the wt% H_2O content for each sample calculated using the water equation

[8]the actual wt% H_2O of the sample calculated via FTIR spectroscopy

[9]the iterative correction factor calculated for Rhyolitic, Dacitic, and Trachytic glasses

[10]the wt% H_2O content for each sample after application of the correction factor

Table 7: Uncertainties in calculated water content

Sample #	Calculated H_2O (wt%)[1]	True H_2O (wt%)[2]	Difference[3]	Average[4]
1-8-6 B	3.43	2.68	0.75	0.85
1-9-10 A	5.37	5.94	0.57	
1-9-10 B	4.83	4.32	0.51	
1-10-1 A	3.21	2.27	0.94	
1-10-1 B	2.89	2.45	0.44	
1-10-2 A	4.50	3.93	0.57	
1-10-2 B	5.33	5.35	0.02	
1-10-15 A	2.96	4.25	1.29	
1-10-15 B	3.15	3.98	0.83	
1-10-15 C	3.09	3.37	0.28	
1-13-10	3.81	5.99	2.18	
1-13-21	7.57	6.59	0.98	
1-14-9 A	6.99	5.44	1.55	
1-15-4	4.34	3.38	0.96	
T 1-4-13	4.57	5.34	0.77	
T 1-5-6	6.42	5.34	1.08	

[1]the wt% H_2O content for each sample after application of the correction factor

[2]the actual wt% H_2O of the sample calculated via FTIR spectroscopy

[3]the absolute value of the difference between the calculated vs. true H_2O values

[4]the average uncertainty for all glasses in wt% H_2O

4.4 Raman analysis of fluorescing inclusions

4.4.1 Anhydrous samples

As detailed in section 3.6.1, a spectral subtraction of a hydrous vs. anhydrous fluorescent glass will leave only the hydrous components behind. This will allow us to quantify the effects of fluorescence on the peak areas of our spectra, and may give insight as to whether our Raman peaks are "riding" atop the fluorescence background, or being obscured by it. The results of this analysis are shown in *Table 8*, which shows that the water content derived for the subtracted (non-fluorescent) values are higher than the original (fluorescent) values. This suggests that the fluorescence background is partially obscuring the water band at ~3600cm^{-1}, reducing its total area during deconvolution and ultimately causing water values to be underestimated. Note however, that the sample size for this experiment was quite small, with only 2 anhydrous analogues made for subtraction. As such, these larger water values might be coincidental. For future studies, a larger suite of samples should be made into anhydrous glasses and tested, to confirm the validity of this claim.

Table 8: Calculated peak-areas and H_2O content (wt%) using subtracted spectra

Sample #	T-O area[1]	Water area[2]	Calc H_2O[3]	Corrected H_2O[4]	True H_2O[5]
T 1-4-13	168	1009	1.86	5.20	5.34
T 1-4-13 subbed	200	1482	2.30	6.43	5.34
1-10-15 A	451	2915	1.20	3.20	4.25
1-10-15 A subbed	446	3204	1.33	3.57	4.25

[1]the sum of all Gaussian peaks between ~700 and ~1250 cm^{-1}

[2]the sum of all Gaussian peaks between ~3000 and ~3800 cm^{-1}

[3]the wt% H_2O content for each sample calculated using the water equation

[4]the actual wt% H_2O of the sample calculated via FTIR spectroscopy

[5]the wt% H_2O content for each sample after application of the correction factor

4.4.2 UV spectroscopy

As mentioned previously, UV excitation is a proven method to mitigate sample fluorescence, and thus remove the fluorescent background from a spectra (Millen et al., 1999 and Severs et al., 2007). As such, three of our fluorescent samples, encompassing the full compositional suite of our glasses (rhyolitic, dacitic, and trachytic), were analyzed via UV spectroscopy. *Figure 20* shows a comparison of a UV spectra vs a 532nm (green, visible light) spectra. The fluorescent background is completely eliminated from the UV spectra, giving an unobstructed view of both the T-O and water band regions.

Table 9 and *Figure 21* show a comparison of the final water values determined by our 532nm Raman method, and our UV method. Curiously, there is little difference between the calculated water contents of the UV and 532 analytes, which still fall within 0.85 wt% of the true H_2O content. This suggests that the water and T-O bands in our fluorescent spectra are relatively unaffected by the fluorescence background, and can produce accurate peak areas for water determination without any special treatment. It is important to note, however, that UV Raman spectra may appear different from normal Raman spectra, as many compounds can absorb UV radiation (Smith, 2005). This has been shown to alter the relative intensities of Raman bands. This calls into question whether it was appropriate to use the calibration derived from our 532nm glasses to our UV glasses. For future studies, a wider range of glasses may be compared between UV and light microscopy, to assess if the fluorescent background can be truly ignored, or if it requires treatment.

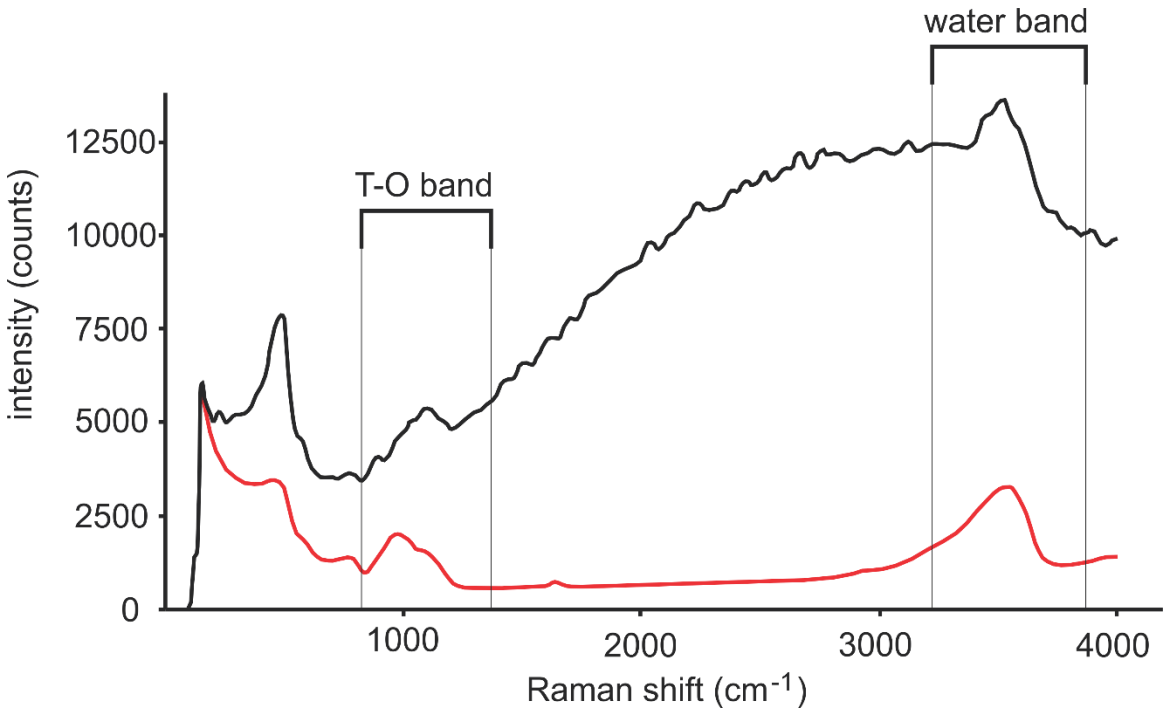

Figure 20: UV (red) vs. 532nm (black) spectra for sample T 1-4-13.

Table 9: UV excited spectra (405nm) and 532nm spectra from HORIBA Scientific (H_2O values in wt%)

Sample #	Laser wavelength[1]	T-O area[2]	Water area[3]	Calc H_2O[4]	Corrected H_2O[5]	True H_2O[6]
1-10-15 A	405	2638	28576	2.00	5.03	4.25
1-10-15 A	532	2441	23937	1.82	4.94	4.25
1-15-4	405	2959	11161	2.01	4.10	3.38
1-15-4	532	3747	15117	2.15	5.87	3.38
T 1-4-13	405	1847	17222	2.90	6.04	5.34
T 1-4-13	532	3882	25245	2.02	5.51	5.34

[1]wavelength of the incident laser light

[2]the sum of all Gaussian peaks between ~700 and ~1250 cm^{-1}

[3]the sum of all Gaussian peaks between ~3000 and ~3800 cm^{-1}

[4]the wt% H_2O content for each sample calculated using the water equation

[5]the wt% H_2O content for each sample after application of the correction factor

[6]the actual wt% H_2O of the sample calculated via FTIR spectroscopy

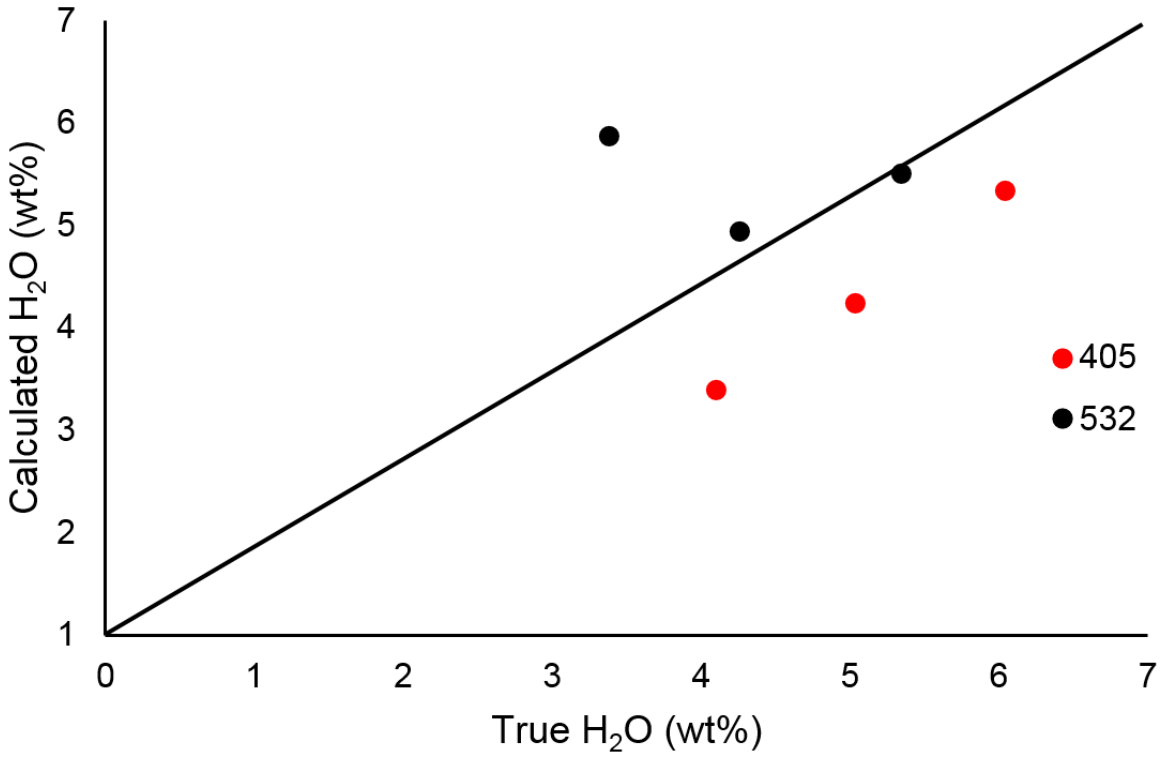

Figure 21: Plot of UV (405 nm) vs. 532nm excitation source derived water contents.

4.5 First test on natural melt inclusions

The methods outlined in sections 3.2-3.5 were applied to natural melt inclusions from southern New Brunswick. These samples were mounted in thin section rather than resin to allow for location of glass inclusions via light microscopy. *Figure 22* shows a typical glass inclusion selected for Raman analysis. *Table 10* shows the average bulk composition of the melts, based on EMP and LA-ICP-MS by Gray et al., (2011). *Table 11* shows the water content of the inclusions derived from our Raman analysis. These H_2O values, on average, fall within 0.70 wt% of their actual values, which demonstrates that the calibration method described in this paper can be applied to natural melt inclusions, as well as bulk glass samples.

The water values derived from our melt inclusion analysis ranged from 0.34 to 3.99wt% H_2O. This range in water content may reflect the position of the Cherry Hill unit as it ascended through the country rock, trapping melt inclusions with decreasing H_2O content as pressure, and thus water solubility, decreased. *Figure 23* shows a plot of our melt H_2O contents on a P-T projection of water solubility modeled for rhyolitic melts (Yamashita, 1999). This projection shows that the maximum depth of entrapment for the Cherry Hill pluton corresponds to a pressure of ~100-120 MPa (or ~50-60 MPa if our 3.99wt% H_2O inclusion is an outlier). This translates to a depth of ~4.07 km (or ~2.04 km) in the crust. The melt inclusions with the lowest H_2O content (1.14-0.34 wt% H_2O) represent a depth of entrapment of ~0.37km (~10MPa). As such, we can surmise that the rhyolitic magma of the Cherry Hill unit lost ~3.65 (or 2.28) wt% H_2O as it traveled from its initial depth of emplacement at ~4.07 (or ~2.04) km to its final depth of ~0.37 km. As such, the dewatering

history of the Cherry Hill magma has been reconstructed using H_2O values derived using Raman spectroscopy.

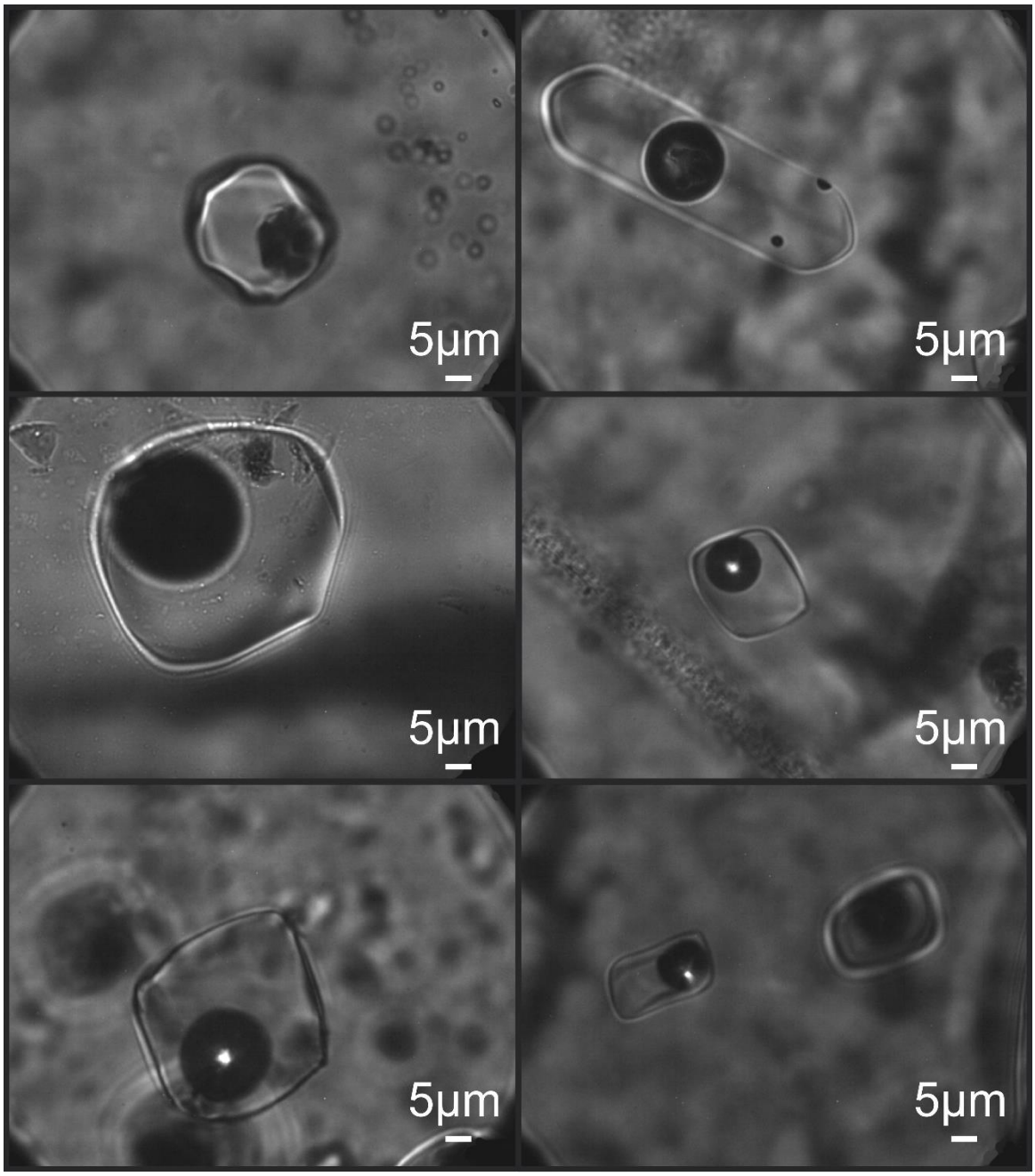

Figure 22: Natural glass inclusions from southern New Brunswick, sample NB07-18.

Table 10: Average bulk composition of NB07-18 melt inclusions (wt%)

SiO_2	73.52
TiO_2	0.089
Al_2O_3	14.46
Cr_2O_3	-
Fe_2O_3	-
FeO	1.26
MnO	0.051
MgO	0.031
CaO	0.822
Na_2O	3.35
K_2O	5.27
H_2O	0.78-1.7

Table 11: Cherry Hill water equation parameters (H_2O values in wt%)

Sample #	T-O pos.[1]	T-O area[2]	Water area[3]	Ttot (FeO)[4]	T tot (Fe_2O_3)[5]	Calc H_2O[6]	True H_2O[7]	Correction Factor[8]	Corrected H_2O[9]
0	1160	64442	68974	1.51	1.53	0.127	0.78-1.7	2.68	0.34
1	1020	94252	68438	1.51	1.53	0.427	0.78-1.7	2.68	1.14
5	1160	63184	103280	1.51	1.53	0.195	0.78-1.7	2.68	0.52
9	1080	28583	67167	1.51	1.53	0.909	0.78-1.7	2.68	2.44
11	1080	46497	101766	1.51	1.53	0.847	0.78-1.7	2.68	2.27
12	1080	58964	70923	1.51	1.53	0.465	0.78-1.7	2.68	1.25
13	1090	35640	98464	1.51	1.53	0.976	0.78-1.7	2.68	2.62
15	1020	33441	84732	1.51	1.53	1.489	0.78-1.7	2.68	3.99
17	1080	43997	40984	1.51	1.53	0.360	0.78-1.7	2.68	0.97

[1]the position of the maxima of the T-O band region

[2]the sum of all Gaussian peaks between ~700 and ~1250 cm^{-1}

[3]the sum of all Gaussian peaks between ~3000 and ~3800 cm^{-1}

[4]the total number of T-site cations in the sample using ferrous Fe in the determination

[5]the total number of T-site cations in the sample using ferric Fe in the determination

[6]the wt% H_2O content for each sample calculated using the water equation

[7]the actual wt% H_2O of the sample calculated via FTIR spectroscopy

[8]the iterative correction factor calculated for Rhyolitic, Dacitic, and Trachytic glasses

[9]the wt% H_2O content for each sample after application of the correction factor

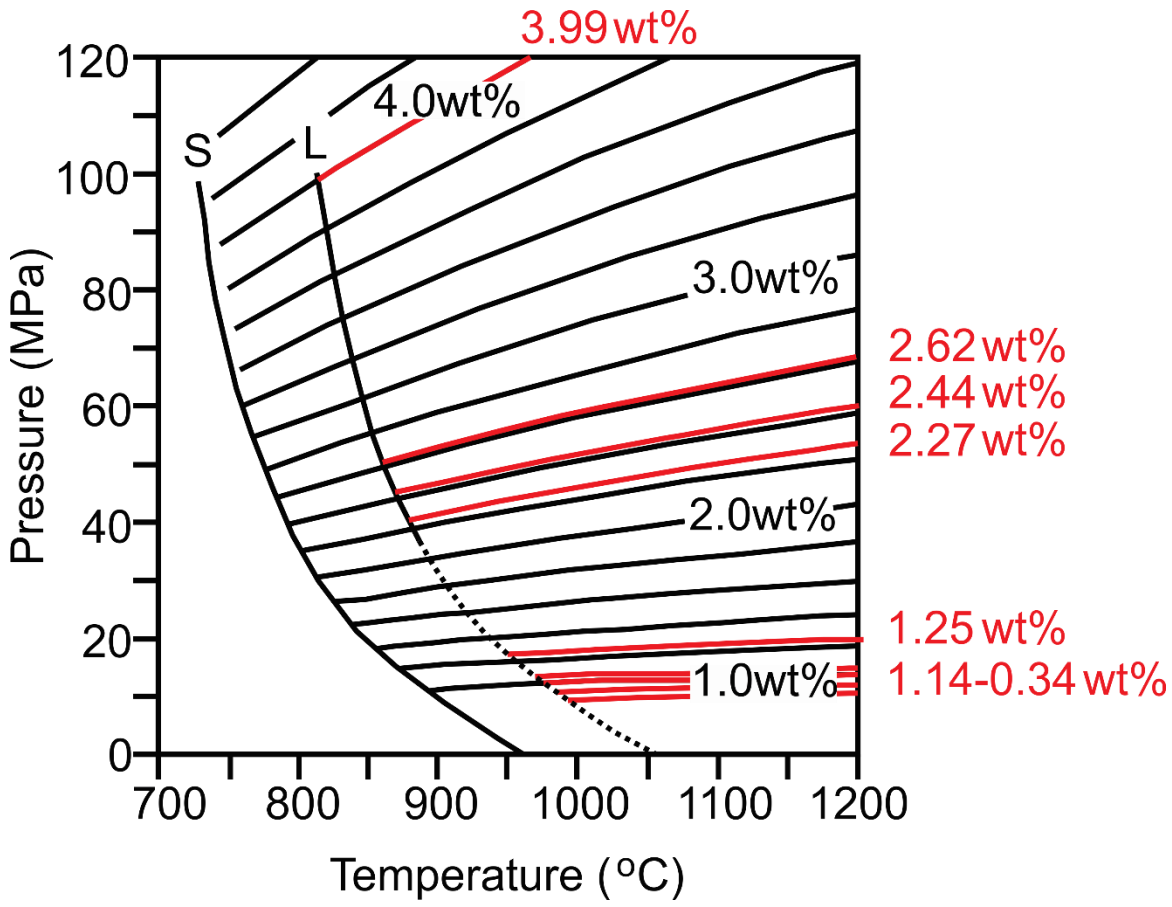

Figure 23: Plot of calculated H_2O contents on a P-T trajectory diagram of water solubility modeled for rhyolitic melts (adapted from Yamashita, 1999).

5.0 Conclusion

Numerous analytical techniques are available for the quantification of water content in silicate glasses (FTIR, ICPMS, SIMS). However, these methods have serious drawbacks in terms of ease of use, sample destruction, and/or analytical uncertainty in deriving water content. Raman spectroscopy has been demonstrated as a quick, non-destructive technique in which water content may be analyzed within rhyolites, dacites, and trachytes to within 0.85 wt% accuracy. The peak-area ratio between the water band at ~3600cm^{-1} and the T-O band at 700-1250cm^{-1} was found to closely approximate H_2O content after application of the baseline and frequency temperature corrections to the spectra, along with special considerations for T-O band variability made in Zajacz et al.s (2005) water equation. The methods described were successfully applied to natural silicate melt inclusions, confirming the versatility of the Raman technique. The largest source of error in the experiment was identified as a combination of glass heterogeneity and variations in the baseline correction of the spectra. This revealed an uncertainty of ± 0.52, 0.48, and 0.96 wt% H_2O for rhyolitic, dacitic, and trachityc glasses respectively. The problems associated with fluorescing spectra, variations in the baseline correction, and sample homogeneity were also addressed and found to be acceptable in terms of the error inherent to the experiment.

Future studies may wish explore other techniques at reducing fluorescence. For example, Smith (2005) states that fluorescence caused by impurities in the sample may be "burned off" if left in the laser beam for some time. In addition, calibration standards based on fluorophores have been proposed for spectrometers in the visible light range. Pulsed lasers have also been found to reduce or mitigate fluorescence.

6.0 References

Burnham, W., 1979. Magmas and hydrothermal fluids, In: Barnes, H.L. (Ed.), Geochemistry of Hydrothermal Ore Deposits, 1st ed. John Wiley and Sons Ltd., New York. 71–136.

Lange, R., 1994. The effect of H_2O, CO_2, and F on the density and viscosity of silicate melts. In: Carroll, M.R., Holloway, J.R. (Eds.), Reviews in Mineralogy, vol. 30. *Mineralogical Society of America*. 331–369.

Ingerson, E., 1950. The Water Content of Primitive Granitic Magma. *American Mineralogist*. 35, 806-815.

Hedenquist, J., Lowenstern., J., 1994. The role of magmas in the formation of hydrothermal ore deposits. *Nature*. 370, 519 - 527

Thomas, R., 1994. Estimation of the viscosity and the water content of silicate melts from melt inclusion data. *European Journal of Mineralogy*. 6, 511-535

Thomas, R., Kamenetsky, V., Davidson, P., 2006. Laser Raman spectroscopic measurements of water in unexposed glass inclusions. *American Mineralogist*. 91, 467–470.

Zajacz Z., Halter, W., Malfait, W., Bachmann, O., Bodnar, R., Hirschmann, M., Mandeville, C., Morizet, Y., Muntener, O., Ulmer, P., Webster, J., 2005. A composition-independent quantitative determination of the water content in silicate glasses and silicate melt inclusions by confocal Raman spectroscopy. *Mineral Petrology*. 150, 631–642

Chabiron, A., Pironon, J., 2004. Characterization of water in synthetic rhyolitic glasses and natural melt inclusions by Raman spectroscopy. *Contributions to Mineral Petrology*. 146, 485–492

Behrens, H., Roux, J., Neuville, D., Seimann, M., 2006. Quantification of dissolved H_2O in silicate glasses using confocal microRaman spectroscopy. *Chemical Geology*. 229, 96–112

Thomas R., 2000. Determination of water contents of granite melt inclusions by confocal laser Raman microprobe spectroscopy. *American Mineralogist*. 85, 868–872.

Mercier, M., Di Muro, A., Giordano, D., Metrich, N., Lense, P., Pichavant, M., Scaillet, B., Clocchiatti, R., Montagnac, G., 2009. Influence of glass polymerisation and oxidation on micro-Raman water analysis in alumino-silicate glasses. *Geochimica et Cosmochimica Acta*. 73, 197–217

Le Losq, C., Neuville, N., Moretti, R., Roux, J., 2012. Determination of water content in silicate glasses using Raman spectrometry: Implications for the study of explosive volcanism. *American Mineralogist*. 97, 779–790

Severs, M., Azbej, T., Thomas, J., Mandeville, C., Bodnar, R., 2007. Experimental determination of H_2O loss from melt inclusions during laboratory heating: Evidence from Raman spectroscopy. *Chemical Geology*. 237, 358–371

Campbell, I., Dickinson, J., Dingwell, D., Dunn, J., Fleet, M., Herzberg, C., Mysen, B., Navrotsky, A., Nicholls, J., Russel, J., Scarfe, C., Stout, M., Turner, J. (1986). Short Course in Silicate Melts. *Mineralogical Association of Canada*. 97

Payette, C., and Martin, R.F., (1986). The Harvey volcanic suite, New Brunswick. II. Postmagmatic adjustments in the mineralogy and bulk composition of a high-fluorine rhyolite. *Canadian Mineralogist*. 24, 571-584

Gray, T., Hanley, J., Dostal, J., Guillong, M. (2011). Magmatic enrichment of uranium, thorium, and rare earth elements in Late Paleozoic rhyolites of Southern New Brunswick, Canada: Evidence from silicate melt inclusions. *Economic Geology*. 106, 127-143.

Bottomley, D. (1984). Origins of some arseniferous groundwaters in Nova Scotia and New Brunswick, Canada. *Journal of Hydrology*. 69, 223-257

Harvey Station (Cherry Hill) Fluorite (2016). Industrial Minerals Summary Data. Government of New Brunswick Geoscience Database. http://www1.gnb.ca/0078/GeoscienceDatabase/IndustrialMinerals/qryIndMinSummary-e.asp?Num=637

Webster, J., Goldoff, B., Shimizu, N. (2011). C–O–H–S fluids and granitic magma: how S partitions and modifies CO2 concentrations of fluid-saturated felsic melt at 200 MPa. *Contributions to Mineral Petrology*. 162, 849-865

Webster, J., Goldoff, B., Sintoni, M., Shimizu, N. De Vito, B. (2014). C-O-H-Cl-S-F volatile solubilities, partitioning, and mixing in phonolitic-trachytic melts and aqueous-carbonic vapor ± saline liquid at 200MPa. *Journal of Petrology*. 55, 2217-2248

Zhang, Z., Chen, S., Liang, Y., Liu, Z., Zhang, Q., Ding, L., Ye, F., Zhou, H. (2009). An intelligent background-correction algorithm for highly fluorescent samples in Raman spectroscopy. *Journal of Raman Spectroscopy*. 41, 659–669

Wojdyr, M. (2010). Fityk: a general-purpose peak fitting program. *Journal of Applied Crystallography*. 43, 1126-1128

Smith, E., Dent, G., 2005. Modern Raman Spectroscopy– A Practical Approach. John Wiley & Sons Ltd, The Atrium, Southern Gate, Chichester, West Sussex PO19 8SQ, England.

Millen, R., Temperini, M., de Faria, D., Batchelder, N. (1999). Raman spectra of poly (2 pyridiniumhydrochloride-2-pyridylacetylene). *Journal of Raman Spectroscopy*. 30, 1027.

Adar, F. (2013). Considerations of grating selection in optimizing a Raman spectrograph. *Spectroscopy*. 28, 10

Wieboldt, D. (2010). Understanding Raman spectrometer parameters. *Spectroscopy*. http://www.spectroscopyonline.com/understanding-raman-spectrometer-parameters

Di Muro, A., Villemant N., Montagnac, G., Scaillet, B., Reynard, B. (2006). Quantification of water content and speciation in natural silicic glasses (phonolite, dacite, rhyolite) by confocal microRaman spectrometry. *Geochimica et Cosmochimica Acta*. 70, 2868–2884

Yamashita, S. (1999). Experimental study of the effect of temperature on water solubility in natural rhyolite melt to 100 MPa. *Journal of Petrology*. 40, 1497-1507